



Trans. Nonferrous Met. Soc. China 35(2025) 579-601

Transactions of Nonferrous Metals Society of China

www.tnmsc.cn



Preparation technology research progress of high-purity antimony

Zong-bo LI^{1,2}, Yan FENG^{1,2}, Yu-feng WEN³, Ri-chu WANG^{1,2}, Xiang PENG^{1,2}

- 1. School of Materials Science and Engineering, Central South University, Changsha 410083, China;
 - 2. National Key Laboratory of Science and Technology on High-strength Structural Materials, Central South University, Changsha 410083, China;
 - 3. School of Mathematical Sciences and Physics, Jinggangshan University, Ji'an 343000, China

Received 30 June 2024; accepted 20 December 2024

Abstract: High-purity antimony (Sb) is essential for industries like semiconductors and photovoltaics, driving research on its production. This review summarizes research advances in production and preparation techniques for high-purity Sb. Three process flowcharts to produce high-purity Sb are described according to different raw materials. Various process parameters of vacuum distillation, zone refining purification techniques and research progress in the field of high-purity Sb are discussed. Numerical simulation, atomic scale simulation, and research progress of alloying elements in the field of high-purity Sb are highlighted. It is shown that for the difficult removal of As element in Sb, the addition of Al makes the regional refining process more effective in reducing the arsenic content. Finally, the purification of high-purity Sb is summarized, providing insights into achieving efficient and environmentally friendly high-purity Sb production and outlining future directions.

Key words: high-purity Sb; preparation technique; purification; segregation

1 Introduction

Sb is a member of group VA in the periodic table, belonging to the same group as As and Bi, and is typically considered a semimetal or metalloid [1,2]. Due to its scarce reserves, non-renewable nature, widespread applications, irreplaceability, and strategic importance in military applications, Sb, along with rare earth elements, W, and Sn, constitutes one of the four strategic resources in China [3–5]. In terms of elemental abundance in the Earth's crust, Sb ranks the 63rd. Furthermore, Sb resources are unevenly distributed globally. This uneven distribution, coupled with its critical role in multiple key areas, makes Sb an element of significant strategic value [6]. Sb is a silver-white metal that is toxic, brittle, and lacking

ductility, but it possesses excellent corrosion resistance. Sb and its compounds are extensively used in a variety of applications, such as flame retardants, semiconductors, military industries, pharmaceutical and chemical industries, glass production, pigments, memory devices, and thin-film solar cells. For a detailed list of uses and application fields of Sb and its compounds, refer to Table 1 [7–11].

There are over a hundred Sb minerals in nature, among which stibnite (Sb₂S₃) is the primary ore mineral source of Sb [12]. The global distribution of Sb resources is uneven, mainly concentrated in several key regions: the Mediterranean region, the circum-Pacific belt, and the Tian Shan orogenic belt in Central Asia [13]. Table 2 [14] shows the global distribution of Sb resources. By 2021, the total identified Sb resources worldwide exceeded 2×10⁶ t.

Table 1 Application of Sb and its corresponding

compounds [7-11] Material Use and field Sb elementary Si or Ge single crystal doping; substance alloy preparation Catalysts for PET production; Sb₂O₃ flame retardants in plastics, textiles, and rubbers; pigments Sb_2O_5 Flame retardants NaSbO₃, Flame retardants, and decolorants NaSb(OH)₆ used in optical glass production Lubricants in brake pads, Sb_2S_3 optoelectronic conductors Sb_2S_5 Rubber vulcanizing agents Sb(CH₃COOH)₃ Catalysts for polyester production Infrared detectors InSb Ge₁Sb₂Te₄ Storage Positive grid for lead-acid **PbSb** batteries Light absorber layer for thin film Sb₂Se₃ solar cells Substrate materials for fiber optic GaSb communication devices Bearing alloys, printing alloys and PbSbSn cable sheathing materials SbCl₃, SbCl₅ Fluorocarbon production Photovoltaic cells, and liquid Sb₂O₅/SnO₂ (ATO) crystal displays $K_2Sb_2(C_4H_2O_6)_2 \cdot 3H_2O$ Emetics in medicine ZnSb Lithium-ion battery Sb nanoparticles Sodium-ion battery

Table 2 Reserves of Sb resources in world [14]

C₆H₉O₆Sb

Country	Reserve/10 ⁵ t	Proportion/%		
China	4.8	24.0		
Russia	3.5	17.5		
Bolivia	3.1	15.5		
Kyrgyzstan	2.6	13.0		
Myanmar	1.4	7.0		
Turkey	1.0	5.0		
Australia	1.0	5.0		
Other countries	2.6	13.0		
Total number	>20	100%		

Catalyst

China, Russia, Bolivia, and Kyrgyzstan are the countries with the richest Sb reserves, each possessing more than 10% of the global total reserves. Among these four countries, China has the most abundant Sb resources, with reserves reaching 4.8×10⁵t, accounting for 24% of the global total reserves, ranking the first in the world [15]. China's Sb resources are characterized by abundant reserves, large scale, favorable mineralization environments, and relatively concentrated Sb deposits [16]. China's Sb resources are distributed across 18 provinces and autonomous regions, particularly concentrated in the following six provinces and autonomous regions: Hunan, Guangxi, Guizhou, Yunnan, and Gansu. The Sb reserves in these provinces account for 20.4%, 15.9%, 13.5%, 10.5%, 8.8%, and 8.4% of the national total, respectively [14]. Hunan Province leads the country in Sb reserves, with 37 Sb deposits.

According to the data presented in Table 3 [14], China, Russia, and Tajikistan were the top three Sb producing countries from 2015 to 2021. China ranked the first, typically accounting for around 50% of global annual production. From 2015 to 2019, China's annual Sb output remained relatively stable at around 1×105t. The global demand for flame retardants is a major driver of consumption, followed by the lead-acid battery sector [17]. Although China's Sb resources are abundant and production capacity is high, as seen in Table 3, from 2015 to 2022, China's Sb production has shown a decreasing trend year by year. On the one hand, Sb is a scarce resource with low substitutability [9]. On the other hand, the early development of China's Sb industry was not rational [18], often involving rough extraction methods, putting the country's Sb reserve resources at certain risk. Additionally, Sb itself is toxic, and large-scale mining and smelting of Sb release some Sb and harmful substances into the surrounding environment [8,19]. In recent years, increasing attention to ecological environmental protection in China has impacted the Sb production, which is one of the reasons for the decline in Sb output [20].

With the rapid development of high-tech fields such as electronics, information technology, and new energy, the market demand for high-purity Sb has surged [21]. Particularly in the semiconductor industry, an extremely low impurity content is a key factor in ensuring excellent performance and stable

Table 3 Outputs of Sb in world from 2015 to 2022 [14] (t)

Country	2015	2016	2017	2018	2019	2020	2021	2022
China	110000	108000	98000	89600	89000	61000	60000	60000
Tajikistan	8000	14000	14000	15200	28000	13000	13000	17000
Russia	9000	8000	14400	30000	30000	25000	25000	20000
Australia	3700	5000	3120	2170	2030	3900	3400	4000
Bolivia	4200	2670	2700	3110	3000	2600	2700	2500
Turkey	2500	4000	2000	2400	2400	1330	1300	1300
Myanmar	3000	3000	1000	2640	6000	2200	2000	4000
Others	1600	3300	1780	1880	1570	1970	4600	1200
Total	142000	148000	137000	147000	162000	111000	112000	110000

operation of semiconductor devices [22-24]. The production of high-purity Sb metal involves both chemical and physical methods [22]. Chemical methods primarily include multi-stage extraction and electrolytic refining techniques [25], while physical methods encompass directional solidifriction [26], vacuum distillation [27,28], and zone refining [29,30]. Since a single technique is often insufficient to achieve the required high-purity of Sb metal, a combination of chemical and physical methods is typically employed [31]. Chemical methods offer high flexibility and selectivity during the purification process but generally can only purify Sb metal to a 4-5 N purity level. By integrating physical purification techniques such as vacuum distillation and zone refining, the purity of Sb metal can be further enhanced to 7 N or higher [32]. This study aims to analyze and summarize the latest research progress in the production and purification technologies for high-purity Sb metal. It explores the process flowcharts for producing high-purity Sb from different feedstocks and methods. including analysis, influencing factors, theoretical impurity distribution models.

2 Progress in preparation of high-purity Sb metal

The techniques for producing high-purity Sb can be broadly categorized into three main approaches based on the feedstock [33,34]: (1) extracting high-purity Sb from Sb compounds; (2) extracting high-purity Sb from industrial-grade pure Sb metal through pyrometallurgical processes; (3) obtaining high-purity Sb through electrolytic

refining techniques. These methods typically leverage the specific properties of Sb or its compounds, employing single refining operations such as recrystallization, distillation, hydrolysis, electrolysis, hydrogen reduction, vaporization, extraction, and zone refining. These operations are rationally combined to target the impurity elements present in the feedstock [32]. In practical production, chemical and physical methods are often used in combination to achieve optimal purification effects. Whether chemical or physical methods are employed, the typical approach involves selecting the most effective single refining process for initial purification, followed by zone refining techniques to obtain high-purity products [35]. For Sb purification, this approach is particularly crucial. The initial refining step aims to remove the bulk of impurities, while subsequent zone refining further enhances the purity to the desired level.

2.1 Extracting high-purity Sb from Sb compounds

One method for extracting high-purity Sb from antimony compounds involves the use of SbCl₅ [36]. Using SbCl₅ as a raw material, it is first treated with dry HCl gas to produce HSbCl₆·1/2H₂O. This compound crystallizes into fine crystals upon cooling. These crystals are separated and dissolved in a small amount of water. By repeating this process multiple times, HSbCl₆·1/2H₂O can be purified. The purified antimony chlorate solution is diluted with a large amount of water and heated to promote hydrolysis, forming a precipitate. Subsequently, the precipitate is washed with hot water to remove residual chlorine, and impurities are removed through

filtration and drying steps. Finally, using either hydrogen or potassium cyanide as a reducing agent, the antimony compound is reduced to obtain high-purity metallic Sb.

The process for producing high-purity Sb from industrial-grade Sb oxide is shown in Fig. 1. The core of this process lies in first preparing high-purity SbCl₃, then hydrolyzing SbCl₃ to obtain a white precipitate containing Sb₂O₃ and Sb₄O₅Cl₂. Next, distillation purification is performed in a vacuum environment at a temperature below the melting point of SbCl₃ to further purify the product. Finally, through hydrogen reduction technology, high-quality high-purity Sb can be obtained. It is worth noting that, whether using high-purity Sb oxide or lower quality Sb oxide produced by pyrometallurgy as raw materials, distillation purification can yield SbCl₃ with a purity exceeding 5N, providing a reliable raw material basis for the subsequent process. If necessary, zone refining is also performed on the high-purity Sb to produce ingots, resulting in the final product.

High-purity Sb can be prepared through the conversion process of SbCl₃, as detailed in the process flowchart shown in Fig. 2. This method [37] is particularly effective for removing As impurities,

which are commonly present and difficult to eliminate from Sb. The principle is based on the different boiling points and vapor pressures of the chlorides of Sb and its impurities at the same temperature, allowing separation by distillation. First, pre-distillation is carried out at temperatures ranging from 473 to 493 K to remove water, hydrochloric acid, and some low boiling-point impurities. Then, distillation at around 493 K is performed to evaporate and separate SbCl₃, while high boiling-point impurities remain in the residue, resulting in high-purity SbCl₃. This process begins with the reaction of metallic Sb with Cl₂ or SbO₃ with hydrochloric acid to generate SbCl₃, followed by distillation to obtain pure SbCl₃. Unlike the process shown in Fig. 1, which prepares high-purity Sb from SbCl₃, the process in Fig. 2 directly reduces the obtained SbCl₃ with hydrogen, rather than first preparing SbCl₃. Additionally, there is a another process where 10 wt.% of pure water is added to the distilled SbCl₃, followed by hydrogen reduction at temperatures between 1073 and 1173 K, yielding high-purity Sb with a purity exceeding 5 N [38]. One advantage of this method is that the high-purity SbCl₃ obtained through distillation does not leave the system, thereby avoiding potential

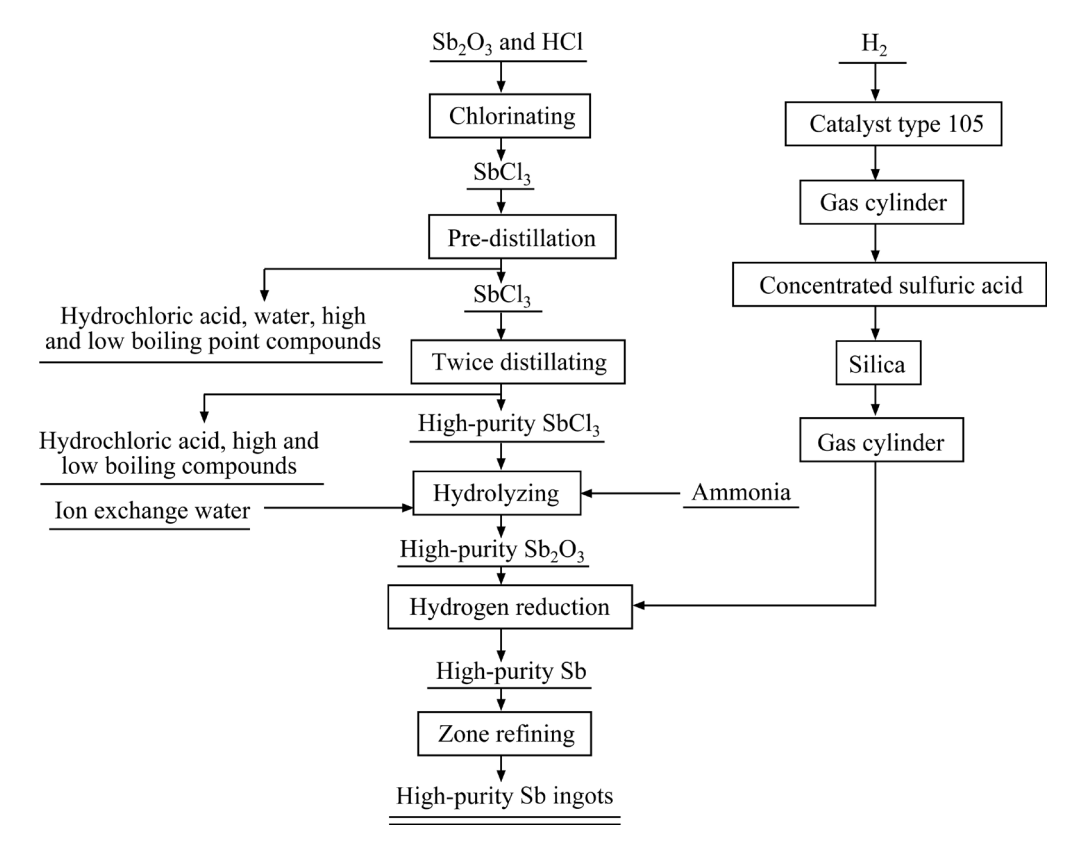


Fig. 1 Process flowchart of high-purity Sb by hydrogen reduction of SbCl₃

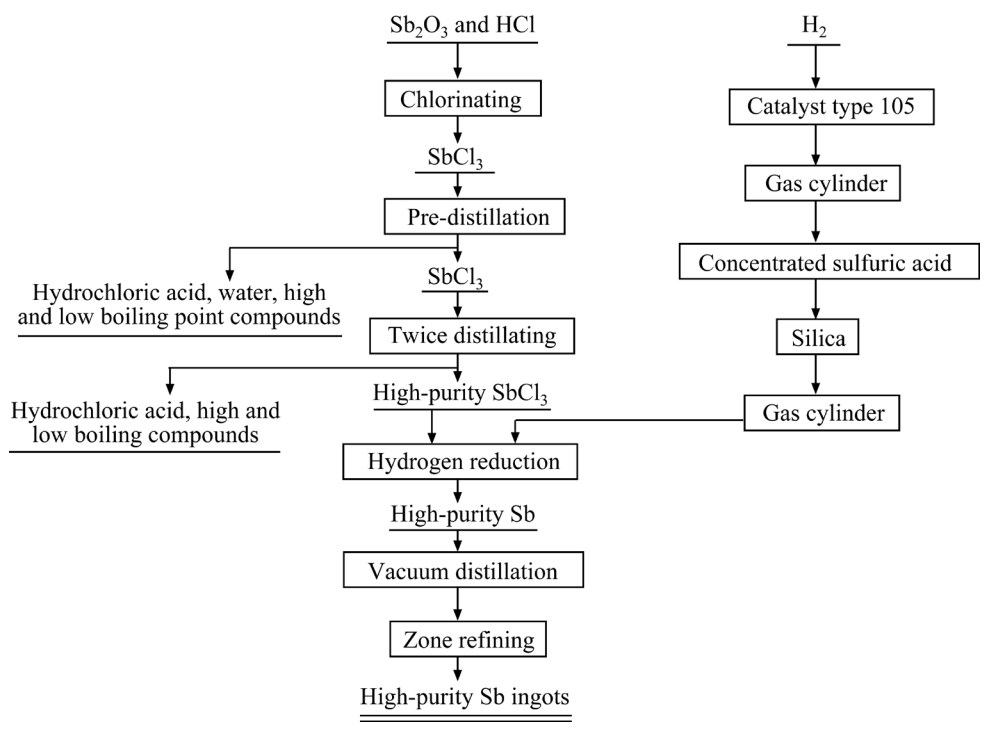


Fig. 2 Process route for preparation of high-purity Sb by distillation-hydrogen reduction of SbCl₃

contamination risks. Currently, many factories employ this process in actual production.

2.2 Preparation of high-purity Sb by purification of refined Sb

Currently, there are two main methods for directly preparing high-purity Sb from refined Sb: vacuum distillation of industrial pure metal Sb and the fumigation method of 4 N Sb [36,39,40]. According to Refs. [36,41], the vacuum distillation method can produce high-purity Sb with a purity of over 5 N. However, due to the high melting point (1908 K) of Sb and its strong corrosiveness in the molten state, it easily forms intermetallic compounds with various metals. This makes the choice of materials for smelting equipment challenging. Particularly in industrial production, as the equipment scales up, the requirements for materials become stricter. The 4N Sb fumigation method is a technology used by the Xifengshan Antimony Refinery of China. This method uses 4N Sb as the raw material and involves two fumigation processes, two reduction smelting processes, and alkaline refining to remove arsenic. High-purity Sb is then obtained through vacuum distillation and zone refining. The process flowchart is shown in Fig. 3. The main purpose of fumigation is to remove lead and iron. Nevertheless, the arsenic content remains high. By adding pure soda, arsenic

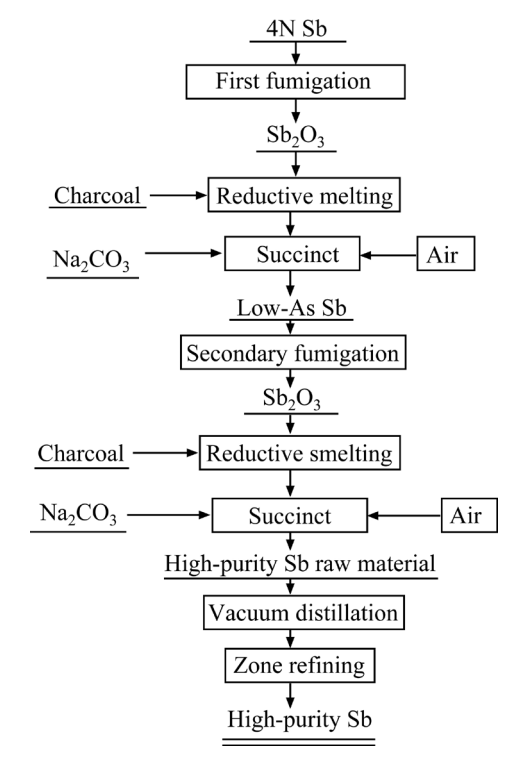


Fig. 3 Process flowchart of 4N-Sb fumigation method to produce high-purity Sb

is oxidized to arsenic pentoxide and removed. After two fumigation and alkaline refining processes, the raw material undergoes vacuum distillation to remove mechanical inclusions and some metal impurities, achieving the separation of high boilingpoint impurities such as copper, iron, gold, and silver from Sb. The product from vacuum distillation is further purified by zone melting, where the primary role of zone melting is remelting.

Additionally, some researchers have tried adding 15%–20% sodium carbonate to industrial-grade Sb to create slag, stirring at 1173–1203 K, and then standing at 1023 and 1073 K to remove the slag. The obtained Sb is placed in a graphite crucible, using a key as the condenser, filtered through a copper mesh, and distilled in a vacuum to produce low-As pure Sb [36]. However, this method mainly removes As from Sb and is limited in removing other impurities. The purity of the resulting product still cannot reach above the 4N standard.

2.3 Preparation of high-purity Sb from Sb electrolytic refining

High-purity Sb can be produced through an electrolytic process, which can be divided into acidic and alkaline electrolytic refining methods [36,42]. In the acidic electrolytic refining process, Sb₂O₃ is first dissolved in industrial-grade HCl. The solution is heated to 381 K to remove the azeotrope of HCl and water, simultaneously eliminating As impurities. At 473 K, SbCl₃ is separated through distillation. SbCl3 is then prepared into an electrolyte with the following composition: 400 g/L SbCl₃ (Sb content); 1.5 mol/L HCl; 3.3 mol/L H₂SO₄. During the electrolysis process, the temperature is maintained at 298-305 K, and the current density is controlled at 10-15 A/m². Spectroscopically pure 5N graphite is used as the anode, while a Pt sheet serves as the cathode. This electrolytic method enables the production of high-purity Sb with a purity exceeding 5N. The alkaline electrolytic refining of high-purity Sb is conducted in a two-stage process [14,43]. Initially, a sulfide-alkaline electrolyte is used to produce Sb at the cathode, which is then remelted to serve as anodes for the second stage. In the second stage, an electrolyte composed of NaOH, Na₃CO₂, and xylitol is employed for electrolysis. The Sb obtained from the cathode is subjected to 4 to 5 rounds of zone refining to yield Sb with a purity exceeding 4N. An alternative method involves hydrolyzing distilled SbCl₃ in ammonia water to form Sb₂O₃, which is then dissolved in a mixed solution of sorbitol and NaOH. Electrolysis is carried out using a nickel-plated titanium mesh as an inert anode in a temperature range of 313–343 K, with a cell voltage of 3–5 V and a current density of 150–400 A/m² [32,36,39]. The advantage of this method is the reduced contamination due to the use of a nickel-plated titanium anode, as opposed to the use of graphite, which can flake off and contaminate the cathodic Sb during electrolysis. Moreover, this method offers higher production efficiency and less stringent requirements for the electrolyte composition and electrolysis temperature compared to the two-stage process.

The current processes for producing highpurity Sb metal have their unique characteristics and limitations. The electrolytic method is favored for its high yield and convenience in industrial production [44-46], but the purity of the Sb produced typically ranges between 4N and 5N. Additionally, the electrolysis process can generate highly toxic gases such as AsH₃ and SbH₃, posing significant safety risks [47]. In laboratory settings, methods for directly preparing high-purity Sb from industrial-grade refined Sb have been explored. However, the high requirements for equipment materials and the challenges of industrialization limit their widespread application. In industrial practice, a more common and widely recognized process involves purifying SbCl₃ through distillation of the chloride of antimony, followed by hydrogen reduction. This method is considered a classic process for producing high-purity Sb metal, capable of achieving purities of 5N or even 6N.

3 Research progress on purification methods for high-purity Sb metal

The preparation of high-purity materials typically requires the integrated use of multiple purification techniques to ensure the effective removal of impurities. Common purification techniques include vacuum distillation [48], zone refining, directional solidification, and solid-state electromigration, among others [49,50]. Each technique has its unique advantages and limitations, often targeting specific types of impurities for removal. In the production of high-purity Sb, a diversified purification strategy that combines physical and chemical methods is employed [27,32]. For instance, methods such as vacuum distillation,

zone refining, and electrolytic refining can be used in combination. The combined use of these processes can complement each other, enhance the purification efficiency, and ensure the acquisition of high-purity Sb materials.

3.1 Vacuum distillation

3.1.1 Fundamental principle

Vacuum distillation is a technique for metal purification based on the differences in saturated vapor pressures of different substances [51,52]. It offers advantages such as simple operation, environmental friendliness, and high raw material utilization, and has been widely applied in the production of high-purity metals. Figure 4 [32] provides a schematic diagram of a vacuum distillation furnace, which helps to visually understand its structure and operating principles. In the vacuum distillation process, when the solid phase and gas phase reach equilibrium, the resulting vapor pressure is called the saturated vapor pressure, or simply vapor pressure [53]. Different substances have varying vapor pressures, and these pressures change with temperature. Figure 5 [32] illustrates the vacuum distillation process high-purity Sb metal, further explaining the implementation steps and principles purification technique.

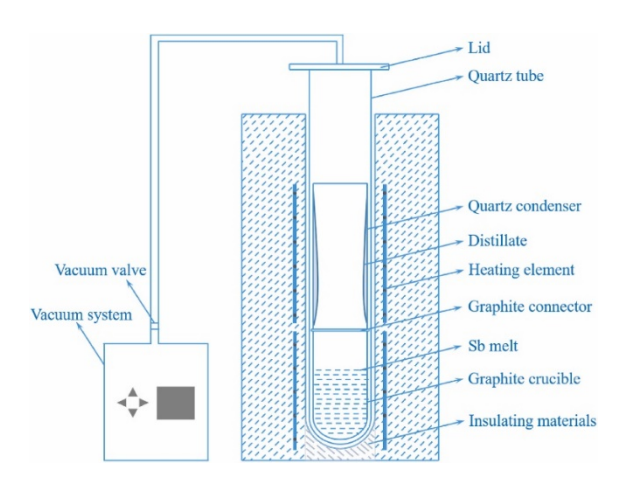


Fig. 4 Schematic diagram of vacuum distillation furnace [32]

3.1.2 Basic equations for vacuum distillation

Generally, substances with higher saturation vapor pressures are more prone to evaporate and transition into the gas phase, whereas those with lower saturation vapor pressures tend to concentrate within the liquid melt [53,54]. The relationship

between the saturation vapor pressure of a metal and temperature can be described by the following formula [32,55,56]:

$$\lg p^* = AT^{-1} + B\lg T + CT + D \tag{1}$$

where A, B, C, and D are specific constants derived from parameters in related literature. These constants are related to the saturation vapor pressure (p*) of each component and the temperature T.

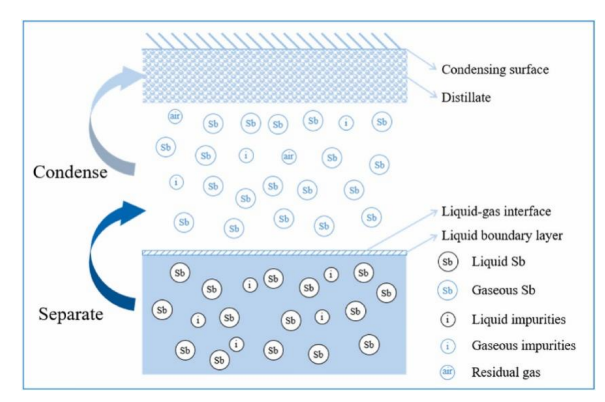


Fig. 5 Schematic diagram of Sb and impurity migration during vacuum distillation process [32]

The separation coefficient at the equilibrium of gas—liquid phases can be used to qualitatively assess whether impurities can be separated from the main metal using vacuum distillation and the ease of such separation [32,41]. The calculation equation is expressed as follows:

$$\beta_{\rm A} = (\gamma_{\rm A} p_{\rm A}) / (\gamma_{\rm B} p_{\rm B}) \tag{2}$$

where β_A is the separation coefficient of component A, γ_A and γ_B are the activity coefficients of components A and B, respectively, which are related to the composition of the components and the state in which the system is located, and p_A and $p_{\rm B}$ are the saturated vapor pressures of components A and B, respectively. Generally, if β_A is less than 1, the component A tends to be enriched in the melt during distillation with only a small amount of volatilization into the gas phase. Conversely, if β_A is greater than 1, then component A tends to volatilize into the gas phase during distillation. If β_A is close to 1, it is difficult to separate components A and B by vacuum distillation. Figure 6 [41] shows the relationship between the vapor pressures of various components in crude Sb and temperature.

3.1.3 Research status

At present, a substantial body of research has been dedicated to the extraction of high-purity Sb

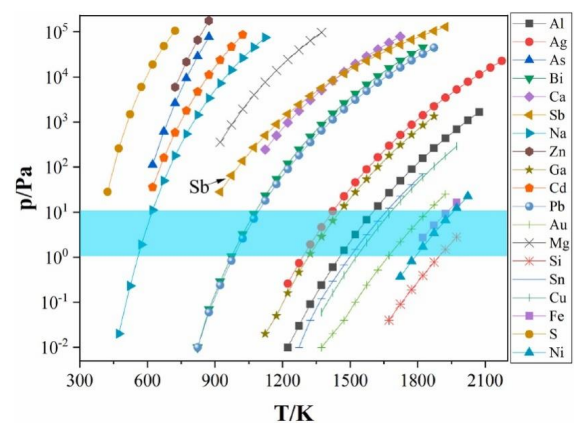


Fig. 6 Variation of saturation vapor pressure for constituents in crude Sb with temperature [41]

using vacuum distillation methods. MENG et al [41] used a custom-built vertical vacuum furnace with heating, vacuum, cooling, and temperature measurement systems to investigate the effects of temperature and holding time on impurity removal. Two main purification methods include low temperature-high temperature vacuum distillation (LHVD) and high temperature-low temperature vacuum distillation (HLVD). For LHVD, in the first stage at 773-873 K low boiling point impurities are removed, and in the second stage at 923-1173 K high boiling point impurities are removed. For HLVD, in the first stage at 923-1173 K high boiling point impurities are removed, and in the second stage at 773-873 K low boiling point impurities are removed. Their main findings are: the LHVD process achieved a higher purity of 99.9961% Sb with 39×10⁻⁶ total impurities; the HLVD process achieved a purity of 99.9947% Sb with 52.94×10⁻⁶ total impurities. The LHVD process had better removal rates for Bi (77.20%) and Cd (27.82%), while the HLVD process had a better removal rate for Zn (83.51%). Figure 7 [41] illustrates the LTVD process, highlighting the impact of two critical factors: the effect of distillation temperature on the process, and the influence of the soaking time on the outcome.

The previous studies have shown significant differences in impurity concentrations in the distillate, leading to unclear average impurity concentrations in the final distilled product [57]. To address this, ZHENG et al [57] developed a model to quantitatively predict the average concentrations of high and low volatile impurities in the distillate during vacuum distillation of Sb metal, in order to

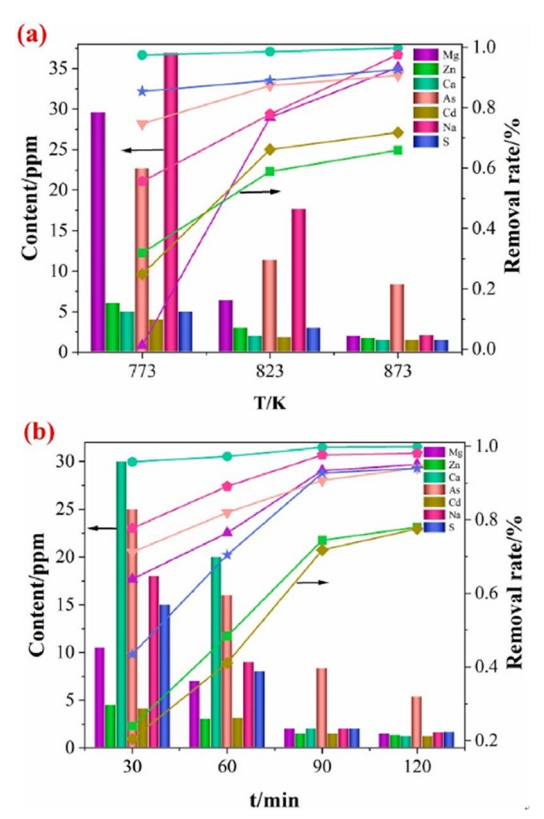


Fig. 7 Process of LTVD: (a) Effect of distillation temperature on process; (b) Influence of soaking time on outcome [41]

ensure the distilled product meeting purity standards. two-section distillation furnace with temperature rise and heat preservation stage was used, the distillates under argon pressure were remelted, impurity concentrations were measured using inductively coupled plasma optical emission spectrometer (ICP-OES), and microstructure and composition were analyzed using the scanning electron microscope and energy dispersive Five spectrometer (SEM-EDS). continuous distillation experiments and two verification experiments were conducted. Figure 8 [57] shows the relationship between the impurity concentration of distillates from different regions in experiment and the SEM micrographs.

The average concentrations of high and low volatile impurities in the distillate during the vacuum distillation process can be depicted by the models developed by the ZHENG et al [57]. Figure 9 [57] shows the saturation vapor pressures of As, Sb, and Bi (Fig. 9(a)) and the evaporation coefficients of As and Bi impurities (Fig. 9(b)). The concentration of As impurity in the residue decreases exponentially during the distillation, while

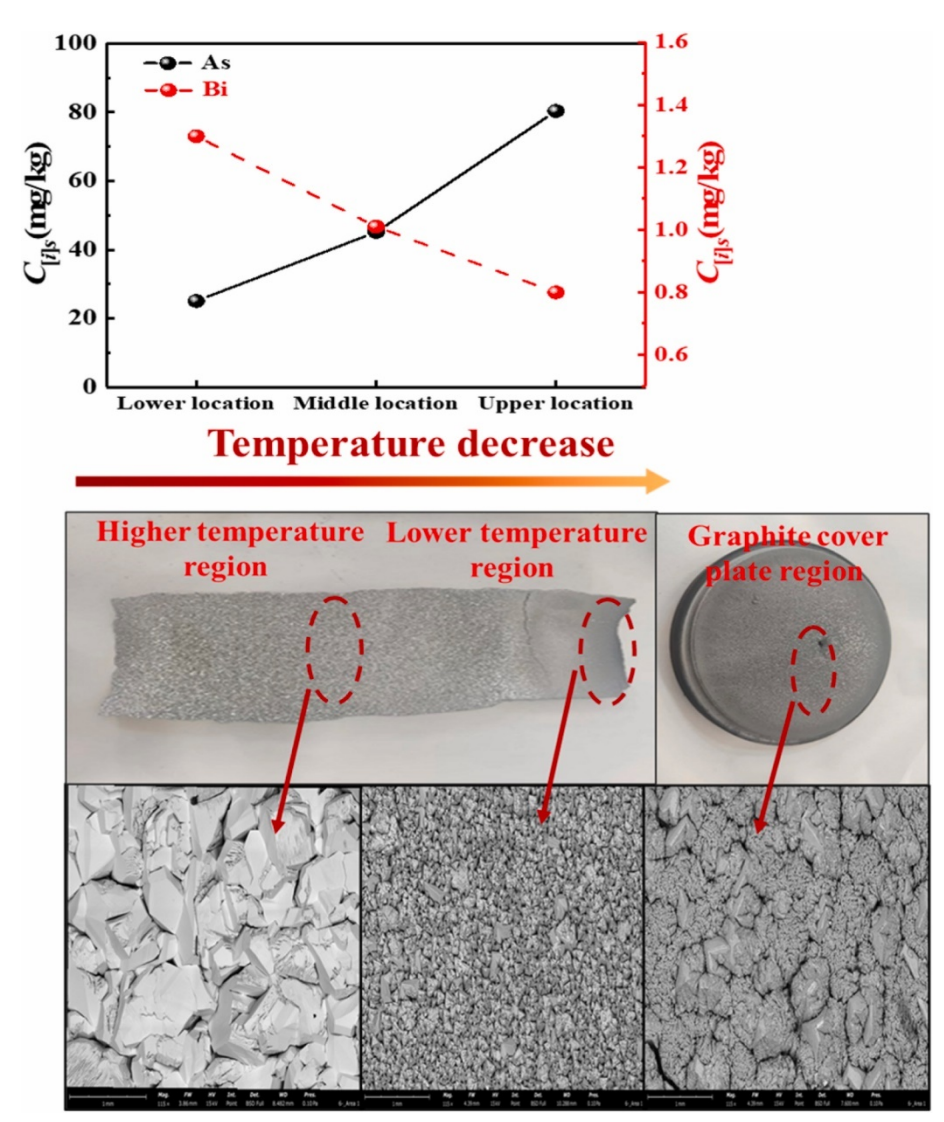


Fig. 8 Relationship between impurity concentration of distillates from different regions in experiment and SEM micrographs [57]

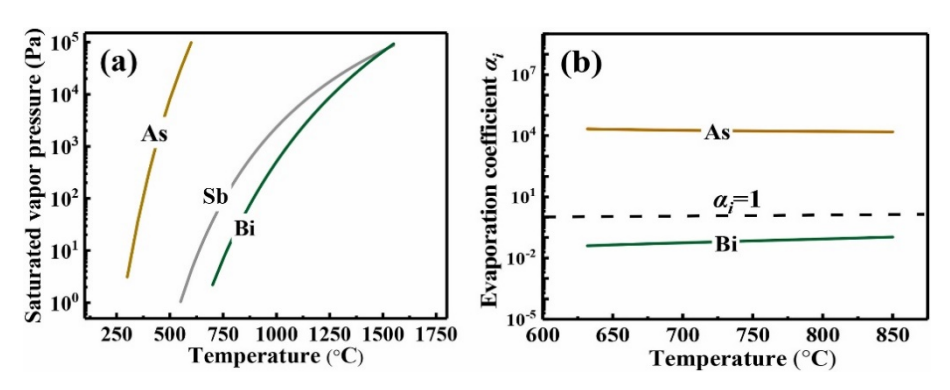


Fig. 9 Saturation vapor pressures of As, Sb and Bi (a), and evaporation coefficients of As and Bi impurities (b) [57]

the concentration of Bi impurity increases exponentially. The models for impurity behavior in the residue and distillate were generally supported by the experimental data, with some deviations [57]. Figure 10 [57] illustrates a comparative analysis of

the dimensionless impurity concentrations in the residue against experimental data.

ZHANG et al [58] proposed a model to describe the behavior of As impurity during the vacuum volatilization purification process of Sb metal with the goal of determining the optimal degree of volatilization and predicting the As impurity concentration in the purified Sb metal. They find that the concentrations of As impurity in both residue and volatile exhibit an exponentially decreasing trend throughout the entire volatilization process. And the decrease in the condensing temperature at the different locations of volatiles leads to an increase in As impurity concentration, which is accompanied by the variation in crystal morphology. Figure 11 [58] shows the scanning electron microscope micrographs of volatiles at different locations. At volatilization degrees of 36.94%, 30.28%, and 47.09%, the As impurity concentration decreases from the initial values to 10 mg/kg, which meets the purity standard of 4.5 N. Figure 12 [58] shows the prediction curves of As impurity concentration in Sb metal purified by vacuum volatilization.

Ab initio molecular dynamics (AIMD) simulations have been proven to be highly reliable in predicting the structural properties of a wide range of materials, encompassing both liquid metals and semiconductors [59–62]. SONG et al [59] studied the structural and electronic properties of liquid Pb–Sb alloys using AIMD, and found that the Pb–15wt.%Sb point is the azeotropic point. The key finding of the research is the identification of the azeotropic point of the Pb–Sb alloy at 15 wt.% Sb, which is supported by both the AIMD simulations and the experimental results [59]. Figure 13 [59] shows the partial pair correlation functions of different compositions in Pb–Sb alloys at 1173 K.

MENG et al [63] performed a study on the evaporation rate and kinetic mechanism of pure and noble Sb under vacuum conditions, using a vacuum differential gravimetric furnace to measure the continuous mass change of the samples at different

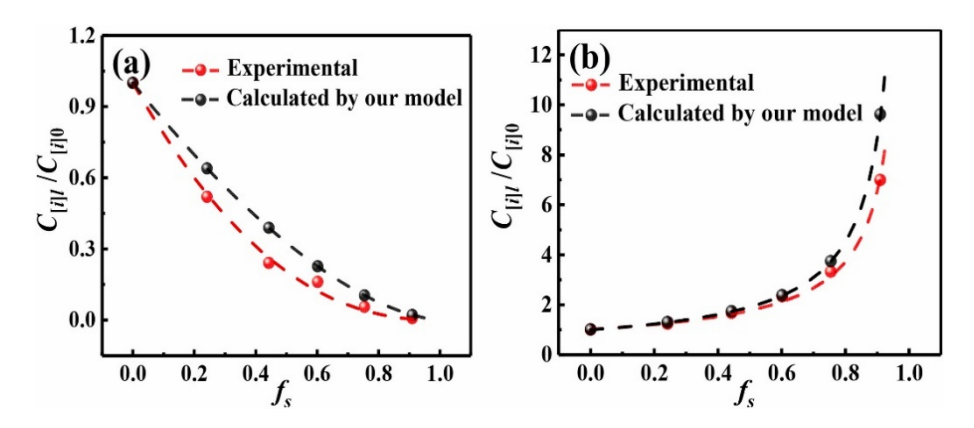


Fig. 10 Dimensionless impurity concentrations in residue against experimental data: (a) As; (b) Bi [57]

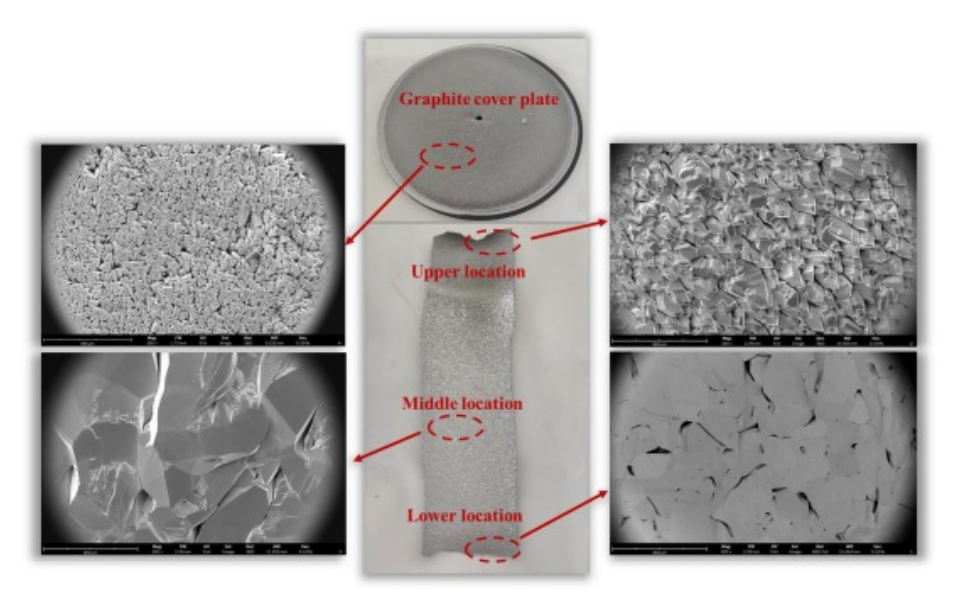


Fig. 11 SEM images of volatiles in different locations [58]

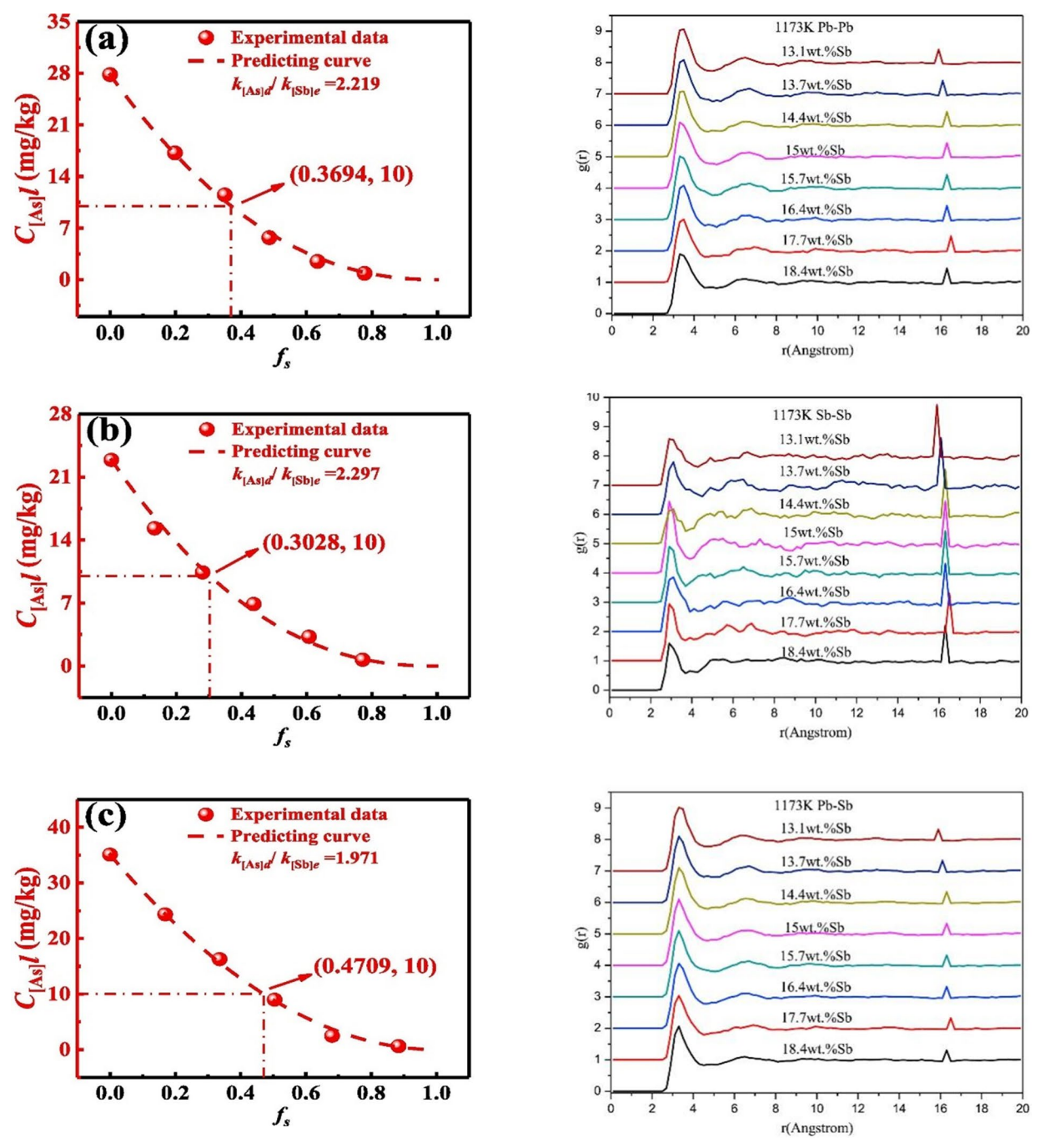


Fig. 12 Predicted concentration curves of As impurities during vacuum volatilization purification of Sb metal at different temperatures: (a) 700 °C; (b) 730 °C; (c) 760 °C [58]

temperatures and pressures, and analyzed the data using mathematical and statistical methods. They found that the actual evaporation rates of pure and noble Sb at 823–1023 K and 5–600 Pa increased with increasing temperature and matched a nonlinear logistic model. And the critical pressure values of pure and noble Sb increased linearly with increasing temperature. The actual maximum evaporation rates of both pure and noble Sb were

Fig. 13 Partial pair correlation functions of different compositions in Pb-Sb alloys at 1173 K [59]

less than the corresponding theoretical maximum evaporation rates, and the evaporation coefficient (α) was less than 1.

Meanwhile, LI et al [32] investigated the variation in contents of Cu, Fe, Ni, Pb, and Bi impurities in Sb melt and distillate during vacuum distillation, establishing models to describe these variation tendencies and finding differences in the mass transfer processes and removal efficiencies of the impurities. Figure 14 [32] shows the theoretical

trends in $k_{\rm eff}$ impurity content across various scenarios. Use a vertical vacuum distillation furnace to purify Sb. Place 4.8 kg of raw Sb material in a graphite crucible inside a quartz tube connected to a quartz condenser. Evacuate the system to below 10 Pa, and then heat the material to 1003.15 K for 35 min. Maintain the pressure at 5–10 Pa, switch to a high vacuum of 10^{-2} – 10^{-1} Pa and distill for 30 min, with the condenser 290 K cooler than the distillation temperature. Collect and analyze the residue and distillate after each run. Repeat the distillation 5 times, with the residue from the previous run as the new raw material.

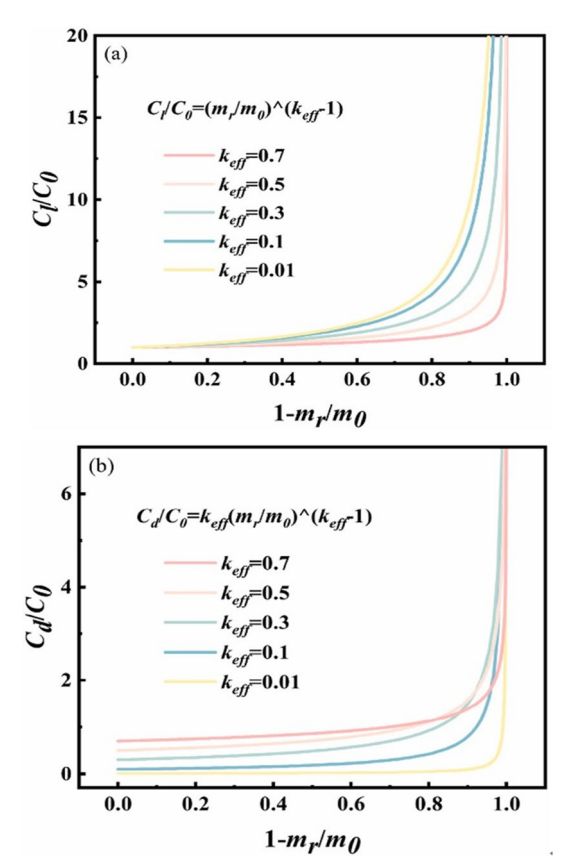


Fig. 14 Theoretical trends in k_{eff} impurity content across various scenarios: (a) In melt; (b) In distillate [32]

It is found that during the vacuum distillation process, the concentrations of impurities such as Cu, Fe, Ni, Pb, and Bi in the Sb melt and distillate exhibit exponential growth. And the rate-determining step is the mass transfer of impurities Cu, Fe, and Ni at the liquid-vapor interface, whereas the transfer of Pb and Bi is governed by a combination of mass transfer processes in the liquid boundary layer and at the liquid-vapor interface. The experimental and computational results for the dimensionless

impurity concentrations in the melt are presented: (a) Cu; (b) Fe; (c) Ni; (d) Pb; (e) Bi. The removal rates of the impurities follow the deceasing order: Cu, Fe, Ni > Pb > Bi, with the Cu, Fe, and Ni impurities having the highest removal rates and the Bi impurity having the lowest rate.

3.2 Zone refining

3.2.1 Fundamental principle

Zone refining is a technique that achieves purification of the primary metal by utilizing the differences in solubility of impurities in the solid and molten states of the main metal [64-66]. This process redistributes solutes, thereby altering the distribution of impurities to purify the primary metal. Zone melting has been applied in the preparation of high-purity materials, i.e., Al [67–69], Cu [61,70,71], In [72], and Sb [73]. Figure 15 [31] shows schematic diagrams of zone melting. Place the metal rod to be purified in a high-purity graphite crucible. Once the heating coil reaches the melting point of the metal, it uniformly and slowly moves from one end of the crucible to the other, completing a single refining cycle. As the coil passes, the metal rod melts, and upon the coil's departure, the metal re-solidifies, causing impurities to migrate and accumulate at the ends of the rod during the melting and solidification process. After multiple refining cycles, by excising the impurityenriched ends, the purified metal is obtained from the central section.

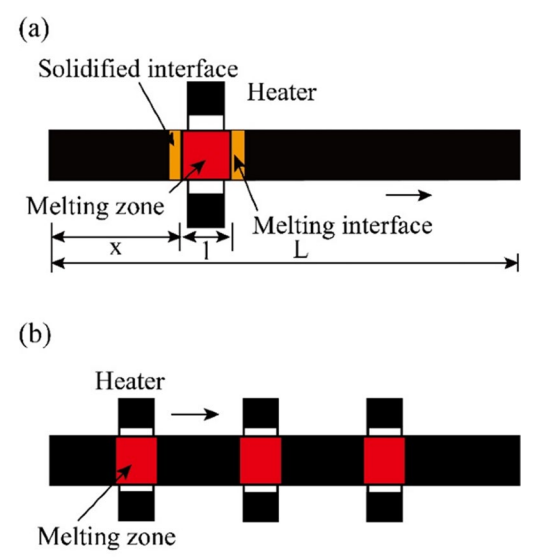


Fig. 15 Schematic diagrams of zone refining process highlighting two distinct approaches: (a) Single-pass zone refining; (b) Multi-pass melting zone refining with iterative cycles [31]

3.2.2 Basic equations for zone melting

The equilibrium distribution coefficient (K_0) and the effective distribution coefficient (K_{eff}) are key factors influencing the efficiency of the purification process and the final purity. The relationship between them can be described by the following equation [31,74]:

$$K_{\text{eff}} = \frac{K_0}{K_0 + (1 - K_0) \exp(-\nu \delta/D)}$$
 (3)

where v is the velocity of the molten zone movement, D is the diffusion coefficient of the impurity in the molten state of the primary metal, and δ is the thickness of the diffusion layer at the solid-liquid interface.

3.2.3 Impact of distribution coefficients on zone melting

The equilibrium K_0 is a core parameter influencing impurity migration and plays a decisive role in the entire separation and purification process. The greater the deviation of K_0 from 1 is, the more significant the effect of zone refining on removing impurities is. When predicting the theoretical distribution of impurities during the zone refining process, the effective distribution coefficient K_{eff} can reflect the actual situation more accurately [31]. For example, CHEUNG et al [75] found that predictions in Sb zone refining based on the distribution coefficient were more effective consistent with experimental data. The distribution of Pb concentration in Sb samples through the zone refining process was analyzed. After 10 zone refining passes, the difference in impurity distribution predicted by the equilibrium distribution coefficient and the effective distribution coefficient could reach two orders of magnitude.

3.2.4 Impact of melting times on zone melting

The efficiency of a single zone melting purification is constrained, necessitating multiple iterations for enhanced purification [76]. The distribution of impurities in the metal rod after successive zone melting processes is illustrated in Fig. 16 [31]. The empirical formula for the number of zone melting iterations (n) is given by n=kL/l (where k is an empirical constant ranging from 1.0 to 1.5, L denotes the length of the metal rod, and l is the width of the melting zone). However, LI and LUO [77] observed in their study on zone refining of high-purity zinc that after 10-20 refining passes, the concentration of most impurities significantly

decreased. When the number of refining passes increased to 20–25, the impurity concentration stabilized. This indicates that once the number of refining passes reaches a certain threshold, further increase has limited effectiveness in improving impurity removal rates. To enhance the efficiency of zone refining, in practical operations, multiple heaters are often evenly spaced along the metal rod to create multiple molten zones simultaneously [78]. This not only effectively reduces the purification time required but also enhances the efficiency of impurity removal.

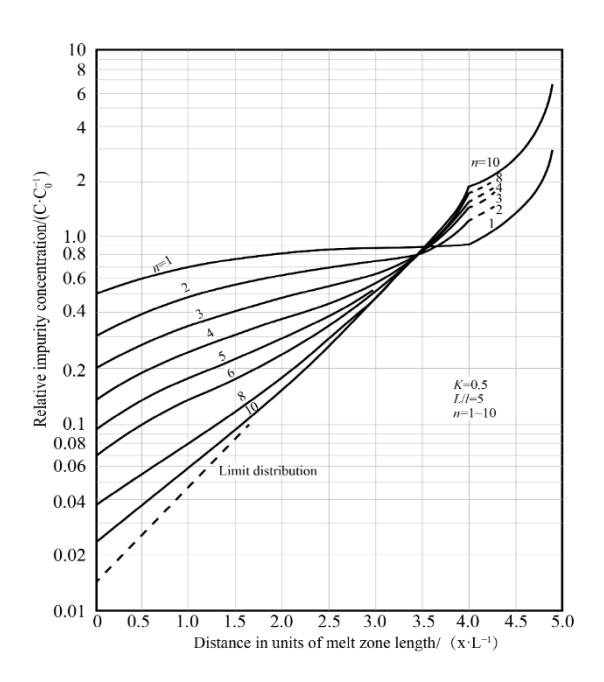


Fig. 16 Relationship between impurity concentration and number of zone refining cycles [31]

3.2.5 Impact of melting zone velocity on zone melting

Equation (3) indicates that for a given zone melting system with known diffusion coefficient D and diffusion layer thickness δ , a reduced melting zone travel rate v leads to the effective distribution coefficient $K_{\rm eff}$ to be closer to the equilibrium distribution coefficient k_0 , enhancing the purification outcome. For instance, PRASAD et al [79] observed a significant reduction in impurity levels during the purification of Te by zone melting. By decreasing the melting zone velocity from 1.0 to 0.75 mm/min, the concentration of Se impurities dropped from 75.65×10^{-6} to 17.69×10^{-6} , and Pb impurities decreased from 4.8×10^{-6} to 1.5×10^{-6} . Upon further reducing the velocity to 0.5 mm/min,

the concentration of Se impurities was further lowered to 13.92×10^{-6} , and Pb impurities to 1.15×10^{-6} . In the purification of Si, MEI et al [80] demonstrated that reducing the melting zone velocity from 10 to 1.0 mm/min can effectively remove the majority of impurities, thus enhancing the purity from 2N to 4N. This suggests that a lower melting zone velocity results in better purification outcomes. However, an excessively low velocity can prolong the purification cycle and decrease production efficiency. Consequently, the optimal selection of the melting zone velocity should balance the purification effectiveness with the reduction of the production cycle.

3.2.6 Impact of molten zone width on zone melting

The width of the molten zone plays a crucial role in determining the distribution of impurities between the liquid and solid phases. This width is influenced by various factors, including the temperature distribution, the speed of the molten zone movement, the thermal conductivity of the crucible, and the consistency of the raw material. When the number of zone refining passes is low, a wider molten zone helps to remove impurities more effectively. Conversely, when the number of zone refining passes is high, a narrower molten zone provides better impurity removal efficiency. By combining the use of wide and narrow molten zone techniques, the efficiency of impurity removal can be significantly enhanced. For example, HUANG et al [81] adopted a strategy of initially using a wide molten zone followed by transitioning to a narrow molten zone during the purification of Ce, thereby enhancing the efficiency of impurity removal in the zone refining process. Selecting the appropriate molten zone width is crucial for purification needs of different metals, varying zone refining passes, and types of difficult-to-remove impurities. HO et al [82] developed a numerical model capable of predicting the optimal molten zone width (1) for different numbers of zone refining passes. This model shows that the optimal molten zone width increases with the increase of the equilibrium distribution coefficient and decreases with the increase of the number of zones refining passes. In cases with a high number of zone refining passes, using a narrow molten zone for purification not only maximizes impurity removal efficiency but also improves the yield of acceptable samples.

3.2.7 Impact of heat source on zone melting

The impact of the heat source during the zone melting process is primarily reflected in the control of the melting zone width and the diffusion interface. A narrow heating device with a rapid temperature rise rate can effectively control the width of the melting zone. The heating methods zone refining include resistance used in heating [83–85], induction heating [86–88], electron beam heating [80,89,90], and plasma arc heating [91], among others. Resistance heating, with its broad application and mature technology, stands as the mainstream technique in current zone refining. Induction heating is primarily utilized for the zone melting of metals or semiconductors with high electrical conductivity. Electron beam heating is mainly applied to the zone melting of certain metals with high melting points, characterized by its controlled melting zone width and pronounced temperature gradient, yet its development is hindered by the stringent requirement of high vacuum conditions. Plasma arc heating [91] boasts advantages such as high heating temperatures and rapid temperature rise, but its complex equipment design and high operational difficulty have limited its widespread application.

3.2.8 Type of zone refining

Zone refining techniques can be categorized into several different types based on their operational methods and application characteristics. All these types are based on the same principle of impurity distribution, and each has its own improvements and specializations. The main types include horizontal zone refining [92], vertical zone refining [93], floating zone refining [94], and continuous zone refining [95]. Horizontal zone refining, due to its mature technology and wide application, is suitable for the purification of most metals. Vertical zone refining, although it occupies less space, has limited applications due to its complex operation and the risk of crucible cracking. Floating zone refining, by moving the molten zone vertically without contact with the crucible, effectively avoids secondary contamination and is particularly effective in removing volatile metal impurities and gaseous impurities. This method is especially suitable for purifying reactive metals. Continuous zone refining has attracted attention for its high production efficiency and low secondary

contamination. However, due to the complex equipment, operational difficulties, and high costs, it is currently still in the research and development stage and has not yet been widely adopted for industrial applications.

4 Application of simulation to purification of high-purity Sb

4.1 Numerical optimization simulation

Numerical simulation plays an important role in optimizing the vacuum distillation process. Through simulation, the behavior of impurities in the distillation process can be predicted, process parameters can be optimized, and purification efficiency can be improved.

ZHENG et al [57] proposed a new method to predict the concentration of impurities in high-purity Sb metal, and experimentally verified the validity of the model. A model for the variation of the average concentration of impurities was developed based on the principle of mass conservation of solutes during vacuum distillation. Five successive distillation experiments of crude Sb metal were carried out to obtain the variation rule of the average concentration of impurities in the distillate, and two validation experiments of vacuum distillation were carried out to verify the model. The results showed that the concentration of As impurities in the residue decreased exponentially with the distillation process, while the concentration of Bi impurities increased exponentially. The concentration gradients of As and Bi impurities in the distillate showed an increasing and a decreasing trend, respectively. With the reduction of the condensation temperature, the average concentrations of As and Bi impurities in the distillate showed a linear decreasing and an exponentially increasing trend, respectively. The average concentrations of As and Bi impurities in the distillate were calculated with the two validation experiments. The calculated average concentrations of As and Bi impurities in the distillate match well with the values of the two validation experiments, confirming the validity of the model. Figure 17 [57] shows the comparison between the calculated and experimental results of the dimensionless average impurity concentration in distillates at different degrees of distillation.

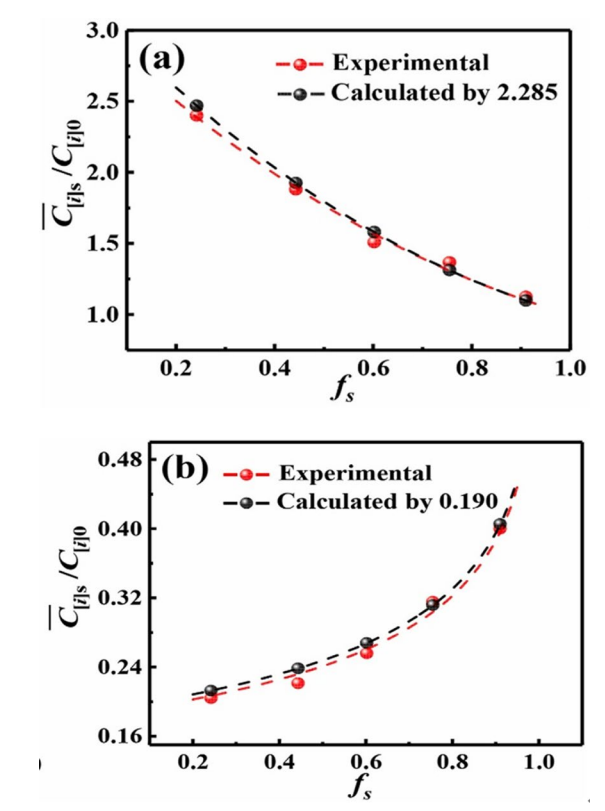


Fig. 17 Comparison between calculated and experimental results of dimensionless average impurity concentration: (a) As; (b) Bi [57]

Zone refining experiments are characterized by long cycles and high energy consumption. Relying solely on traditional experimental methods to study the preparation of high-purity metals is not only time-consuming and energy-intensive but also sometimes even unfeasible. Therefore, developing numerical and simulation models to predict impurity behavior during the zone refining process is crucial for optimizing experimental design and guiding the experimental process.

Modeling for the simulation and optimization of experimental parameters holds significant importance. Building upon the Pfann model, SPIM et al [96] introduced an innovative model that meticulously delineates the impurity distribution zones within a metal rod. The model can analyze the effects of molten zone width, the number of zone passes, and the distribution coefficient K on purification efficiency. Setting the number of zone passes n=5 and the normalized molten zone width Z=10%, impurities will concentrate at both ends of the metal rod after multiple zone passes. By removing sections equal to one molten zone length from each end, a higher purity sample can be

obtained. Using the model to calculate impurity distribution under different experimental conditions allows for the determination of the optimal molten zone width and number of zones passes for specific raw materials, thereby significantly enhancing experimental efficiency and the direct yield of the product.

Additionally, the model can adjust the equilibrium distribution coefficient K_0 of impurities by fitting experimental data. ZHANG et al [29] utilized the Spim model to initially calculate the theoretical distribution of impurities such as Pb, As, and Fe in Sb at various melting zone travel rates. Subsequently, by fitting the experimental data, they revised the equilibrium distribution coefficients to obtain the effective distribution coefficients under specific conditions. For instance, at a melting zone velocity of 2.0 mm/min, the distribution coefficients for Pb, As, and Fe in Sb were 0.33, 0.80, and 0.10, respectively. After correction with the Spim model, these coefficients were adjusted to 0.15, 0.80, and 0.30. It is important to note that in the actual zone melting process, the effective distribution coefficient K_{eff} varies.

4.2 Atomic scale simulation for AIMD

Zone purification utilizes the principle of segregation for purification. It is well known that the segregation process occurs at the solid-liquid interface front. Understanding how solute atoms achieve segregation at the interface is crucial for controlling the segregation process [97–99]. Therefore, it is essential to study the microscopic mechanism of segregation at the atomic scale, understand the kinetics of segregation, and find effective methods to regulate the equilibrium distribution coefficient of solute elements. AIMD calculations can reflect many properties of the melt and provide valuable guidance for practical applications [100-106]. The results of AIMD calculations can clearly indicate the relative strengths of atomic interactions between different species in the melt and can also show the forms in which these atoms are bonded. For example, AIMD simulations on liquid Sb by HAO et al [1] revealed a shoulder in the high wavenumber side of the first peak in the structure factor s(q), indicating residual structural units of crystalline Sb remain in liquid Sb. There is a noticeable bending around 1023 K in the temperature dependence of the first-peak height of s(q), cluster properties, suggesting that an abnormal structural change may occur in the temperature range of 973–1023 K. The evolution of cluster properties implies that structural units with features of crystalline Sb, including Peierls distortion, are present in liquid Sb. But the Peierls distortion weakens and vanishes at around 1023 K.

ZUO et al [107] presented a comprehensive theoretical and experimental study on the separation of As and Sb through a vacuum sublimationgraded condensation process. They adopted thermodynamic analysis and MD simulations to explore the interaction between As and Sb and the behavior of As-Sb clusters in the gas phase. And vacuum sublimation-graded condensation experiments to purify As by separating it from Sb. The thermodynamic and MD calculations show that As and Sb form covalent bonds and clusters during vacuum complicating sublimation. their separation. Different diffusion coefficients and condensation temperatures of the As-Sb clusters can be leveraged to separate them during the vacuum sublimation process. Figures 18(a) and (b) [107] show the mean square displacement (MSD) and diffusion coefficients of As₄, As₃Sb, As₂Sb₂, and AsSb₃. The proposed vacuum sublimation-graded condensation process can effectively remove Sb from crude As, achieving a removal rate of 91.37% under optimized conditions of 748 K, 10 Pa, and 60 min.

Meanwhile, LI et al [108] used the AIMD method to research Sb-X (X=As, Bi, Cu, Fe) local structure and dynamic properties of binary melts. They found that the local structure around As atoms in the Sb melt is the most loose and relaxed compared to Bi, Cu, and Fe. The local structure around Cu and Fe atoms is more ordered and stable compared to As and Bi. The stable and compact local structure around Fe atoms at lower temperatures hinders their diffusion in the Sb melt, leading to its maximum concentration being away from the solid-liquid interface. The loose and unstable local structure around As atoms facilitates their diffusion from the bulk melt to the solid phase, explaining how elements with distribution coefficients close to 1 (like As) can be purified through segregation-based methods.

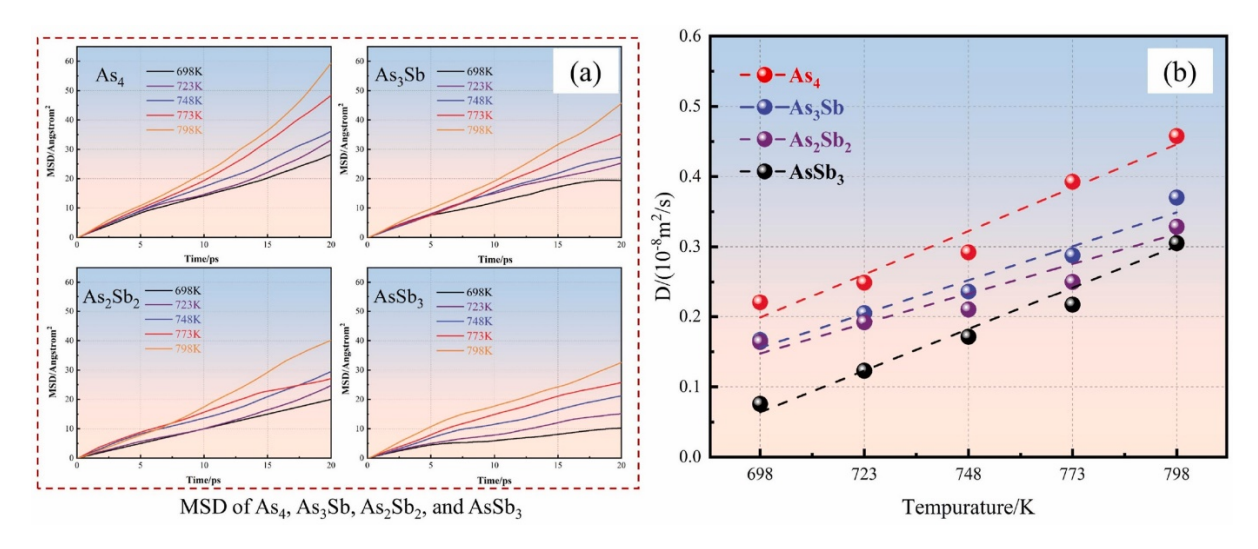


Fig. 18 MSD (a) and diffusion coefficients (b) of As₄, As₃Sb, As₂Sb₂, and AsSb₃ at 698–798 K [107]

5 Influence of alloying elements on purification of high-purity Sb

The segregation method for preparing high-purity Sb is a physical method that solely utilizes the phenomenon of solute redistribution during the metal solidification. However, the purification efficiency of the segregation method is currently not ideal and is affected by inherent defects. Solute elements with an equilibrium distribution coefficient greater than or close to 1 cannot be completely removed by segregation.

For example, the production of solar-grade silicon aims at metallurgical techniques that are low-cost, energy-efficient, and low in pollution. Among the common purification techniques, vacuum distillation is used to remove P, while zone refining is used to remove V, Ti, and Fe. However, the segregation method has limitations in removing B, as the segregation coefficient of B is as high as 0.8 at a temperature of 1687 K [109], making it difficult to effectively remove B through segregation. CHEN et al [110] investigated a method to enhance the removal of B impurities from silicon using an Al-Si solvent with the addition of V, which forms more stable VB₂ compounds. Increasing the amount of V from 0 to 1500×10⁻⁶ increased the B removal rate from 51.9% to 76.8%.

The impurity element As in Sb has an equilibrium distribution coefficient close to 1, making it very difficult to completely remove As

using zone melting. Adding an appropriate small amount of the third element during zone refining can enhance the purification effect [110]. ZHANG et al [73] investigated the separation behavior of As and Pb from Sb during vacuum distillation and zone refining processes, and found that the addition of Al significantly improved the removal of As in both processes. During vacuum distillation process, the addition of 1% Al led to a 67% reduction in the amount of As in the condensate. And a large concentration gradient of As appeared in the residual Sb, indicating the formation of Al-As intermetallic compounds shown in Fig. 19 [73]. For zone refining, the addition of 0.1% Al reduced the As concentration in the entire Sb bar from 456×10^{-6} to below 150×10^{-6} after just one pass, due to the enrichment of Al and the formation of Al-As intermetallic compounds at the end of the bar.

6 Conclusions

This review comprehensively summarizes the production processes of high-purity Sb and the strengths and weaknesses of various purification methods. The aim of this study is to offer theoretical guidance for achieving an efficient industrial production of high-purity Sb. Although there has been extensive expansion in the research and application fields of high-purity Sb, its production and purification still face numerous challenges that require further investigation.

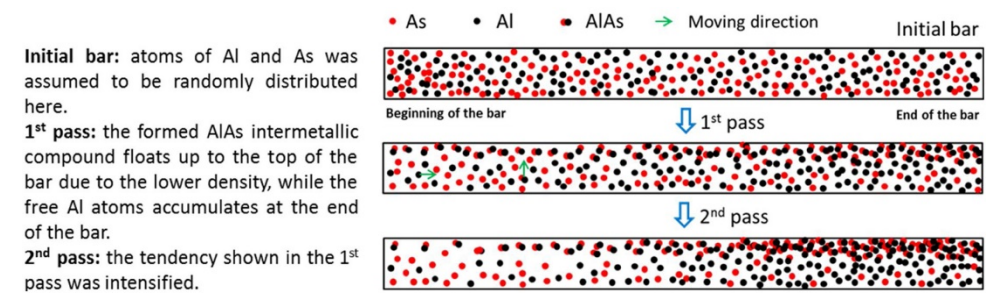


Fig. 19 Schematic diagram illustrating removal of arsenic during zone refining of Sb using aluminum as an additive [73]

The vacuum distillation and zone refining faces challenges in terms of production efficiency and cost. For instance, zone refining requires multiple passes at a relatively slow molten zone travel rate, which extends the production cycle and increases energy consumption. Therefore, exploring ways to improve vacuum distillation and zone refining technology to shorten the process, enhance production efficiency, and reduce costs has become a key research direction. Numerical simulation plays an important role in optimizing vacuum distillation and zone refining processes. Through simulation, the behavior of impurities in the vaccum distillation and zone refining processes can be predicted to optimize the process parameters and improve the purification efficiency. With the deepening of the research, the vacuum distillation and zone melting technologies will be developed in the direction of low-cost, high-efficiency, highreliability and highly targeted industrialization.

To enhance purification efficiency and ensure process stability and reliability, it is necessary to improve single-process methods or integrate multiple purification techniques to develop new processes that are short, efficient, and stable in operation. In the zone refining process, for impurities that are difficult to remove, such as As in high-purity Sb, it is essential to study their migration mechanisms deeply and improve their removal rates. Traditional methods are not ideal for impurities with equilibrium distribution coefficients close to 1. Using AIMD simulations, it is possible to explore the microscopic mechanisms segregation at the atomic scale and understand the dynamics of the process. This research direction is crucial for finding effective methods to regulate the equilibrium distribution coefficient of solute elements. This line of research helps to efficiently

remove some of the impurities that are difficult to remove.

CRediT authorship contribution statement

Zong-bo LI: Validation, Formal analysis, Investigation, Resources, Writing — Original draft, Writing — Review & editing; Yan FENG: Methodology, Conceptualization, Writing — Review & editing, Visualization, Supervision, Funding acquisition, Resources; Yu-feng WEN: Methodology, Conceptualization, Formal analysis, Resources, Supervision, Project administration, Funding acquisition, Resources; Ri-chu WANG: Validation, Formal analysis, Writing — Review & editing; Xiang PENG: Validation, Formal analysis, Writing — Review & editing.

Declaration of competing interest

The authors declare that they have no known competing financial interests or personal relationships that could have appeared to influence the work reported in this paper.

References

- [1] HAO Q H, LI Y D, KONG X S, LIU C S. Ab initio molecular dynamics simulations on local structure and electronic properties in liquid Sb from 913 K to 1193 K [J]. International Journal of Modern Physics B, 2013, 27(5): 1350012.
- [2] GE Rui-guang, SUN Hong-zhe. Bioinorganic chemistry of bismuth and antimony: Target sites of metallodrugs [J]. Accounts of Chemical Research, 2007, 40(4): 267–274.
- [3] QIN Jin, LIU Zheng-qing, TAN Pan, YI Dan-qing, WANG Bin. Study on the formation and regulation mechanism of W phase and the improvement of mechanical properties in homogenization of cast Al-Cu-Sc-Zr alloys: Experiments and calculations [J]. Vacuum, 2023, 207: 111631.
- [4] NI Pei, PAN Jun-yi, HAN Liang, CUI Jian-ming, GAO Yan, FAN Ming-sen, LI Wen-sheng, CHI Zhe, ZHANG Kai-han, CHENG Zhi-lin, LIU Yu-pei. Tungsten and tin deposits in South China: Temporal and spatial distribution, metallogenic

- models and prospecting directions [J]. Ore Geology Reviews, 2023, 157: 105453.
- [5] LI Li-li, DUAN Xue-cheng. Semiconducting of nanocrystalline tin oxide and its influence factors [J]. Transactions of Nonferrous Metals Society of China, 2005, 15(6): 1356–1360.
- [6] ZHAO Gui-mei, LI Wen-xiu, GENG Yong, BLEISCHWITZ R. Uncovering the features of global antimony resource trade network [J]. Resources Policy, 2023, 85: 103815.
- [7] DEMBELE S, AKCIL A, PANDA S. Technological trends, emerging applications and metallurgical strategies in antimony recovery from stibnite [J]. Minerals Engineering, 2022, 175: 107304.
- [8] ZHANG Yang, DING Chun-xia, GONG Dao-xin, DENG Yao-cheng, HUANG Ying, ZHENG Jiang-fu, XIONG Sheng, TANG Rong-di, WANG Yong-chang, SU Long. A review of the environmental chemical behavior, detection and treatment of antimony [J]. Environmental Technology & Innovation, 2021, 24: 102026.
- [9] HENCKENS M, DRIESSEN P, WORRELL E. How can we adapt to geological scarcity of antimony? Investigation of antimony's substitutability and of other measures to achieve a sustainable use [J]. Resources, Conservation and Recycling, 2016, 108: 54–62.
- [10] ANDERSON C G. The metallurgy of antimony [J]. Geochemistry, 2012, 72: 3–8.
- [11] XU Guo-fu, YIN Zhi-min, MOU Shen-zhou, LUO Feng-hua, OIKAWA K. Martensitic and magnetic transformation of Co₄₁Ni₃₂Al₂₄Sb₃ and Co₄₁Ni₃₂Al₂₇ alloys [J]. Transactions of Nonferrous Metals Society of China, 2006, 16(4): 776–782.
- [12] DONG Zhao-wang, GUO Xue-yi, XIONG Heng, LI Ling, XU Bao-qiang. Enriching Sb₂S₃ from jamesonite by one-step vacuum distillation [J]. Vacuum, 2022, 203: 111271.
- [13] KANELLOPOULOS C, SBORAS S, VOUDOURIS P, SOUKIS K, MORITZ R. Antimony's significance as a critical metal: The global perspective and the Greek deposits [J]. Minerals, 2024, 14(2): 121.
- [14] LI Ya-xing. The separation behavior of impurity in antimony during vacuum distillation [D]. Changsha: Central South University, 2023. (in Chinese)
- [15] MOOSAVI-KHOONSARI E, MOSTAGHEL S, SIEGMUND A, CLOUTIER J P. A review on pyrometallurgical extraction of antimony from primary resources: Current practices and evolving processes [J]. Processes, 2022, 10(8): 1590.
- [16] DING Jian-hua, ZHANG Yong, MA Yu-bo, WANG Yan, ZHANG Jian-bin, ZHANG Ting-ting. Metallogenic characteristics and resource potential of antimony in China [J]. Journal of Geochemical Exploration, 2021, 230: 106834.
- [17] MONTSERRAT F. Antimony [M]. Berlin, Boston: De Cruyter, 2021: 73–94.
- [18] HURST C. China's rare earth elements industry: What can the west learn? [R]. Carlisle, Pennsylvania: U.S. Avmy War College, Strategic Studies Institute (SSI), 2010.
- [19] GAN Yong-hai, DING Cheng-cheng, XU Bin, LIU Zhuang, ZHANG Sheng-tian, CUI Yi-bin, WU Bing-dang, HUANG Wen-guang, SONG Xiao-jie. Antimony (Sb) pollution control by coagulation and membrane filtration in water/

- wastewater treatment: A comprehensive review [J]. Journal of Hazardous Materials, 2023, 442: 130072.
- [20] HE Meng-chang, WANG Ning-ning, LONG Xiao-jing, ZHANG Cheng-jun, MA Cong-li, ZHONG Qian-yun, WANG Ai-hua, WANG Ying, PERVAIZ A, SHAN Jun. Antimony speciation in the environment: Recent advances in understanding the biogeochemical processes and ecological effects [J]. Journal of Environmental Sciences, 2019, 75: 14–39.
- [21] DUPONT D, ARNOUT S, JONES P T, BINNEMANS K. Antimony recovery from end-of-life products and industrial process residues: A critical review [J]. Journal of Sustainable Metallurgy, 2016, 2(1): 79–103.
- [22] SCHWARZ-SCHAMPERA U. Antimony [M]. Hoboken, New Jersey John Wiley & Sons. Ltd, 2014: 70–98.
- [23] XU Qi-man, CAO Yu-dong, CHEN Bai-shan, ZHOU Jian, XUE Feng. Revealing the strengthening mechanism of Cu-Sn composites joint fabricated via in-situ reaction for power electronic packaging [J]. Materials Science and Engineering: A, 2024, 895: 146252.
- [24] YU Kun, LI Shao-jun, CHEN Li-san, ZHAO Wei-shang, LI Peng-fei. Microstructure characterization and thermal properties of hypereutectic Si-Al alloy for electronic packaging applications [J]. Transactions of Nonferrous Metals Society of China, 2012, 22(6): 1412–1417.
- [25] MULTANI R S, FELDMANN T, DEMOPOULOS G P. Antimony in the metallurgical industry: A review of its chemistry and environmental stabilization options [J]. Hydrometallurgy, 2016, 164: 141–153.
- [26] SHIGA K, MAEDA K, MORITO H, FUJIWARA K. Facet formation during the solidification of pure antimony [J]. Journal of Crystal Growth, 2022, 586: 126633.
- [27] ZHOU Zhen-tao, DONG Zhao-wang, XIE Hua-xiao, JIANG Wen-long, WANG Yi-zhao, XU Bao-qiang, XIONG Heng, YANG Bin. A novel vacuum distillation method for preparing high purity antimony trisulfide from antimony minerals [J]. Separation and Purification Technology, 2022, 300: 121935.
- [28] DONG Zhao-wang, JIANG Bao-cheng, GUO Xue-yi, XIONG Heng, YANG Bin, XU Bao-qiang, JIANG Wen-long. Separation of mixture of Sb₂S₃-PbS, Sb₂S₃-FeS, PbS-FeS by vacuum distillation [J]. Vacuum, 2023, 214: 112120.
- [29] ZHANG Xiao-xin, FRIEDRICH S, LIU Bin, HUANG Tian-xiang, FRIEDRICH B. Computation-assisted analyzing and forecasting on impurities removal behavior during zone refining of antimony [J]. Journal of Materials Research and Technology, 2020, 9(2): 1221–1230.
- [30] REN Jian, WANG Ri-chu, FENG Yan, PENG Chao-qun, CAI Zhi-yong. Microstructure evolution and mechanical properties of an ultrahigh strength Al–Zn–Mg–Cu–Zr–Sc (7055) alloy processed by modified powder hot extrusion with post aging [J]. Vacuum, 2019, 161: 434–442.
- [31] YU Liang, KANG Xiao-an, CHEN Luo-na, LUO Kun, JIANG Yan-li, CAO Xiu-ling. Research status of high-purity metals prepared by zone refining [J]. Materials, 2021, 14(8): 2064.
- [32] LI Ya-xing, LI Zong-bo, WANG Ri-chu, PENG Chao-qun, FAN Yan, WANG Xiao-feng, CAI Zhi-yong. The separation

- behavior of impurity in antimony during vacuum distillation [J]. Vacuum, 2023, 211: 111669.
- [33] ANDERSON C. SME mineral processing & extractive metallurgy handbook [M]. New Jersey: Engelwood Cliffs, 2019.
- [34] FORTIER S M, NASSAR N T, LEDERER G W, BRAINARD J, GAMBOGI J, MCCULLOUGH E A. Draft critical mineral list Summary of methodology and background information—US Geological Survey technical input document in response to Secretarial Order No. 3359 [M]. New York: US Geological Survey, 2018.
- [35] RAMASWAMY S, HUANG H J, RAMARAO B V. Separation and purification technologies in biorefineries [M]. New York: John Wiley & Sons, 2013.
- [36] GUO Xue-yi, TIAN Qin-hua. High-pure metallic materials [M]. Beijing: Metallurgical Industry Press, 2010. (in China)
- [37] SMITHERINGALE W V. Antimony [M]. Vancover: University of British Columbia, 1925.
- [38] KUBOTA M, KAKEMIZU H. Method for manufacture of antimony of high purity: U.S. Patent, 4629501 [P]. 1986–12–16.
- [39] DENG Ju-hai, ZHANG Yong-wei, JIANG Wen-long, MEI Qing-song, LIU Da-chun. Harmless, industrial vacuum-distillation treatment of noble lead [J]. Vacuum, 2018, 149: 306–312.
- [40] WANG Ai-hua, HE Meng-chang, OUYANG Wei, LIN Chun-ye, LIU Xi-tao. Effects of antimony (III/V) on microbial activities and bacterial community structure in soil [J]. Science of the Total Environment, 2021, 789: 148073.
- [41] MENG Chao-song, YANG Hu-an, WEI Xiao-hui, XU Chang-yi, ZENG Yuan-lin, XIONG Heng, YANG Bin, XU Bao-qiang. A novel process for directional impurity removal and preparation of front-end high-purity antimony from crude antimony [J]. Vacuum, 2024, 219: 112736.
- [42] YANG Jian-guang, WU Yong-tian. A hydrometallurgical process for the separation and recovery of antimony [J]. Hydrometallurgy, 2014, 143: 68–74.
- [43] ZHU Qiang, YANG Jian-guang, NAN Tian-xiang, LIU Jiang, TANG Shi-yang, ZENG Wei-zhi, TANG Chao-bo. Antimony extraction from sulfide concentrates by direct electrolytic desulfurization in molten salt [J]. ACS Sustainable Chemistry & Engineering, 2024, 12(20): 7844–7857.
- [44] CHATENET M, POLLET B G, DEKEL D R, DIONIGI F, DESEURE J, MILLET P, BRAATZ R D, BAZANT M Z, EIKERLING M, STAFFELL I. Water electrolysis: From textbook knowledge to the latest scientific strategies and industrial developments [J]. Chemical Society Reviews, 2022, 51(11): 4583–4762.
- [45] WANG Yi, LIU Biao, WANG Xue-wen, MENG Yu-qi, WANG Xing-ming, WANG Ming-yu. Separation and recovery of Ni from copper electrolyte by crystallization of nickel ammonium sulfate double salt [J]. Transactions of Nonferrous Metals Society of China, 2022, 32(11): 3780–3789.
- [46] JUAN Du, ZHU Hong-qiu, LI Yong-gang, ZHANG Tianming, YANG Chun-hua. Simultaneous determination of trace Cu²⁺, Cd²⁺, Ni²⁺ and Co²⁺ in zinc electrolytes by oscillopolarographic second derivative waves [J].

- Transactions of Nonferrous Metals Society of China, 2018, 28(12): 2592–2598.
- [47] MAYFIELD D B, LEWIS A S, BAILEY L A, BECK B D. Properties and effects of metals [M]. New York: Wiley, 2015: 283–308.
- [48] XU Zhi-peng, JIA Li-li, HE Zhi-qiang, GUO Xue-yi, TIAN Qing-hua. A review of preparing high-purity metals by vacuum distillation [J]. Transactions of Nonferrous Metals Society of China, 2024, 34(5): 1634–1654.
- [49] LIU Hang, ZHANG Yao, LUAN Yi-kun, YU Hui-min, LI Dian-zhong. Research progress in preparation and purification of rare earth metals [J]. Metals, 2020, 10(10): 1376.
- [50] WASEDA Y, ISSHIKI M. Purification process and characterization of ultra high purity metals: Application of basic science to metallurgical processing [M]. Berlin: Springer Science & Business Media, 2002.
- [51] KONG Xiang-feng, YANG Bin, XIONG Heng, LIU Da-chun, XU Bao-qiang. Removal of impurities from crude lead with high impurities by vacuum distillation and its analysis [J]. Vacuum, 2014, 105: 17–20.
- [52] DONG Zhao-wang, GUO Xue-yi, YANG Bin, XIONG Heng, JIANG Wen-long. One-step extracting lead from galena (PbS) by a vacuum distillation method [J]. Vacuum, 2022, 196: 110789.
- [53] ZHA Guo-zheng, WANG Yun-ke, CHENG Ming-qiang, HUANG Da-xin, JIANG Wen-long, XU Bao-qiang, YANG Bin. Purification of crude selenium by vacuum distillation and analysis [J]. Journal of Materials Research and Technology, 2020, 9(3): 2926–2933.
- [54] SHANGGUAN Ming-hui, XIE You-jun, WANG Fan, CHEN Yue, TANG Zhuo, LONG Guang-cheng, XU Sheng-qiao, LI Hui, GAO Ce. Preparation of coatings for moisture migration control of cementitious materials under low-vacuum environment [J]. Materials Letters, 2024, 355: 135553.
- [55] SAFARIAN J, ENGH T A. Vacuum evaporation of pure metals [J]. Metallurgical and Materials Transactions A, 2013, 44(2): 747–753.
- [56] DONG Zhao-wang, LIU Han-ning, GUO Xue-yi, XIONG Heng, YANG Bin, XU Bao-qiang. Volatilization kinetics and thermodynamic stability of antimony sulfide under vacuum conditions [J]. Vacuum, 2023, 213: 112119.
- [57] ZHENG Lin, ZHANG Lei, ZHOU Yi, SUN Yan-rong, NAN Chang-bin, ZHOU Xi-ping, QIN Shi-min, SHI Hua-feng, LI Jia-xuan, XU Bao-qiang. New approach to predict impurity concentration in high-purity antimony metal prepared by vacuum distillation [J]. Vacuum, 2024, 226: 113285.
- [58] ZHENG Lin, ZHANG Lei, LI Jia-xuan, ZHOU Yi, SUN Yan-rong, QIN Shi-min, ZHOU Xi-ping, NAN Chang-bin, XU Bao-qiang, YANG Bin, PAN Jin-gong, FU Gan-hua. Exploring arsenic removal behavior in purification process of antimony metal through vacuum volatilization [J]. Separation and Purification Technology, 2024, 349: 127797.
- [59] SONG Bing-yi, XU Na, JIANG Wen-long, YANG Bin, CHEN Xiu-min, XU Bao-qiang, KONG Lingxin, LIU Da-chun, DAI Yong-nian. Study on azeotropic point of Pb-Sb alloys by ab-initio molecular dynamic simulation and vacuum distillation [J]. Vacuum, 2016, 125: 209-214.

- [60] ZHU Zhuo-ying, DENG Zhi, CHU Ie-keng, RADHAKRISHNAN B, PINGONG S. Ab initio molecular dynamics studies of fast ion conductors [M]//Computational Materials System Design. Berlin: Springer, 2018: 147–168.
- [61] ZHOU Jing, LI Xue-song, HOU Xi-bei, KE Hai-bo, FAN Xing-du, LUAN Jun-hua, PENG Hai-long, ZENG Qiao-shi, LOU Hong-bo, WANG Jian-guo, LIU C T, SHEN Bao-long, SUN Bao-an, WANG Wei-hua, BAI Hai-yang. Ultrahigh permeability at high frequencies via a magnetic-heterogeneous nanocrystallization mechanism in an iron-based amorphous alloy [J]. Advanced Materials, 2023, 35(40): 2304490.
- [62] HU Kun, XIE Rui-wen, SHEN Chen, PENG Hai-long, LIU Hua-shan, ZHANG Hong-bin. High-throughput design of Co-based magnetic Heusler compounds [J]. Acta Materialia, 2023, 259: 119255.
- [63] MENG Chao-song, YANG Huan, WEI Xiao-hui, XIONG Heng, DONG Zhao-wang, YANG Bin, XU Bao-qiang, WU Xiao-song, TANG Zhao-hui, HE Yu-hong. Evaporation rate and kinetic mechanism of noble antimony under vacuum [J]. Separation and Purification Technology, 2025, 352: 128235.
- [64] WU J X, DJAVANROODI F, GODE C, ATTARILAR S, EBRAHIMI M. Melt refining and purification processes in Al alloys: A comprehensive study [J]. Materials Research Express, 2022, 9(3): 032001.
- [65] WANG Bing-feng, CHEN Wei, LI Juan, LIU Zhao-lin, ZHU Xie-bin. Microstructure and formation of melting zone in the interface of Ti/NiCr explosive cladding bar [J]. Materials & Design, 2013, 47: 74–79.
- [66] WANG Bing-feng, XIE Fang-yu, LUO Xiao-zhou, ZHOU Jin-dian. Experimental and physical model of the melting zone in the interface of the explosive cladding bar [J]. Journal of Materials Research and Technology, 2016, 5(4): 333–338.
- [67] WAN He-li, XU Bao-qiang, YANG Bin, ZHAO Jin-yang, DAI Yong-nian. The impurities distribution and purification efficiency of high-purity aluminum preparation by zone melting in vacuum [J]. Vacuum, 2020, 171: 108839.
- [68] REN Jian, MENG Hao, SONG Guang-sheng, SUN Yue-hua, WANG Ri-chu, FENG Yan. Characteristics and microstructure of 7055 Al alloy powder prepared by nitrogen atomization [J]. Transactions of the Indian Institute of Metals, 2024, 77(2): 503–511.
- [69] LV Pin-hui, WANG Ri-chu, PENG Chao-qun, CAI Zhi-yong, FENG Yan, PENG Xiang. The evolution of precipitates and mechanical properties in rapidly solidified 2195 Al-Cu-Li alloy during thermal exposure [J]. Journal of Materials Research and Technology, 2023, 27: 6159-6170.
- [70] PAUL H, CHULIST R, BOBROWSKI P, PERZYŃSKI K, MADEJ Ł, MANIA I, MISZCZYK M, CIOS G. Microstructure and properties of the interfacial region in explosively welded and post-annealed titanium-copper sheets [J]. Materials Characterization, 2020, 167: 110520.
- [71] YAN Shuai-jiang, WANG Ri-chu, PENG Chao-qun, CAI Zhi-yong, PENG Xiang, LV Pin-hui, LI Xin-xing. Microstructural evolution and mechanical properties of the rapidly-solidified and hot-extruded 2196 Al–Li alloy [J]. Journal of Alloys and Compounds, 2024, 988: 174285.

- [72] MINAKOV A, MORIKAWA J, RYU M, ZHURAVLEV E, SCHICK C. Variations of interfacial thermal conductance at melting and crystallization of an indium micro-particle in contact with a solid [J]. Materials & Design, 2021, 201: 109475.
- [73] ZHANG Xiao-xin, FRIEDRICH S, FRIEDRICH B. Separation behavior of arsenic and lead from antimony during vacuum distillation and zone refining [J]. Journal of Materials Research and Technology, 2020, 9(3): 4386–4398.
- [74] SUERFU B, CALAPRICE F, SOUZA M. Zone refining of ultrahigh-purity sodium iodide for low-background detectors [J]. Physical Review Applied, 2021, 16(1): 014060.
- [75] CHEUNG N, BERTAZZOLI R, GARCIA A. Numerical and experimental analysis of an approach based on variable solute distribution coefficients during purification by zone refining [J]. Separation and Purification Technology, 2007, 52(3): 504–511.
- [76] RODRIGUEZ-ROJAS M J, FRIEDRICH S, FRIEDRICH B. Feasibility of employing the cooled finger, a fractional crystallization method for the purification of magnesium [J]. Journal of Sustainable Metallurgy, 2022, 8(3): 1276–1289.
- [77] LI Wen-liang, LUO Yuan-hui. Preparation of high purity zinc by zone refining [J]. Chinese Journal of Rare Metals, 2011, 35(4): 537–542.
- [78] CZERWINSKI F. Modern aspects of liquid metal engineering [J]. Metallurgical and Materials Transactions B, 2017, 48: 367–393.
- [79] PRASAD D S, MUNIRATHNAM N R, RAO J V, PRAKASH T L. Effect of multi-pass, zone length and translation rate on impurity segregation during zone refining of tellurium [J]. Materials Letters, 2006, 60(15): 1875–1879.
- [80] MEI P R, MOREIRA S P, CARDOSO E, CÔRTES A D S, MARQUES F D C. Purification of metallurgical silicon by horizontal zone melting [J]. Solar Energy Materials and Solar Cells, 2012, 98: 233–239.
- [81] HUANG Jun, REN Qing-bo, HU Zu-qi, LIU Xun, MENG Da-qiao. Application of a genetic algorithm to optimize redistribution process in zone refining of cerium [J]. Rare Metal Materials and Engineering, 2017, 46(12): 3633–3638. (in Chinese)
- [82] HO C D, YEH H M, YEH T L. Numerical analysis on optimal zone lengths for each pass in multipass zone-refining processes [J]. The Canadian Journal of Chemical Engineering, 1998, 76(1): 113–119.
- [83] MUNIRATHNAM N, PRASAD D, SUDHEER C, RAO J, PRAKASH T. Zone refining of cadmium and related characterization [J]. Bulletin of Materials Science, 2005, 28: 209–212.
- [84] LEI Guo-peng, WANG Bo, LU Jing, WANG Chen, LI Yi-min, LUO Feng-hua. Microstructure, mechanical properties, and corrosion resistance of continuous heating aging 6013 aluminum alloy [J]. Journal of Materials Research and Technology, 2022, 18: 370–383.
- [85] YUAN Shuo, WU Ming-dong, YIN Xiao, LI Ze-yu, HUANG Yang, XIAO Dai-hong, WANG Juan, HUANG Lan-ping, LIU Wen-sheng. Synchronous improvement of strength and corrosion resistance by an improved variablerate non-isothermal aging process in Al–Zn–Mg–Cu alloy

- [J]. Materials Characterization, 2024, 207: 113491.
- [86] MÜHLBAUER A. History of induction heating and melting [M]. Essen, Germany: Vulkan-Verlag GmbH, 2008.
- [87] GUO Yu-feng, ZHENG Yu, WANG Shuai, XU Fu-chun, CHEN Feng, LI Hao, REN Yu-qiao, WEN Yue-kai, YANG Ling-zhi. Mechanism of iron grains aggregation and growth in metalized pellet under the alternating magnetic fields [J]. Journal of Materials Research and Technology, 2024, 29: 3726–3737.
- [88] SHI Lei, GE Run-qi, TAN Nong-chao, DUAN Xiong-bo, CHEN Jia-jun, ZHOU Tian, SUN Zhi-qiang. Non-contact heating methods of carbon fiber thermoplastic composites based on Joule thermal properties: Optimization and validation [J]. Carbon, 2024, 219: 118830.
- [89] LIU Chuan-lei, WANG Meng, PENG Hai-long, PENG Jian, LIU Hua-shan. Pulse electric current induced interfacial ductile phase on improving the mechanical properties of the Au₂₀Sn/Cu solder joints [J]. Journal of Materials Science: Materials in Electronics, 2024, 35(18): 1210.
- [90] WANG Li-juan, MENG Xiang-peng, ZHANG Jia-ning, WANG Meng, HUANG Cheng-zhi, WANG Xu, JIANG Yan-bin, TANG Ning, MO Yong-da, XIAO Zhu, LOU Hua-fen, ZHOU Li. Accelerated precipitation and enhanced mechanical properties of Cu-3.5Ti alloy via electropulsing treatment [J]. Materials Science and Engineering: A, 2024, 904: 146716.
- [91] MIMURA K, KOMUKAI T, ISSHIKI M. Purification of chromium by hydrogen plasma-arc zone melting [J]. Materials Science and Engineering: A, 2005, 403(1/2): 11–16.
- [92] ROUSSOPOULOS G S, RUBINI P A. A thermal analysis of the horizontal zone refining of indium antimonide [J]. Journal of Crystal Growth, 2004, 271(3/4): 333–340.
- [93] KOLESNIKOV N N, BORISENKO E B, BORISENKO D D, TIMONINA A V. Structure and microstructure of GaTe crystals grown by High-Pressure vertical zone melting [J]. Journal of Crystal Growth, 2013, 365: 59–63.
- [94] SCHWABE D, SCHARMANN A, PREISSER F, OEDER R. Experiments on surface tension driven flow in floating zone melting [J]. Journal of Crystal Growth, 1978, 43(3): 305–312.
- [95] KASHIHARA M, YONETANI H, KOBI T, HYUN S K, SUZUKI S, NAKAJIMA H. Fabrication of lotus-type porous carbon steel via continuous zone melting and its mechanical properties [J]. Materials Science and Engineering: A, 2009, 524(1/2): 112–118.
- [96] SPIM J A, BERNADOU M J S, GARCIA A. Numerical modeling and optimization of zone refining [J]. Journal of Alloys and Compounds, 2000, 298(1/2): 299–305.
- [97] LIU Zheng-qing, QIAN Qi, JIANG Yong, WANG Yi-ren, ZHU Yu-man, NIE Jian-feng. Incoherent tilt grain boundaries stabilized by stacking faults and solute-cluster segregation: A case-study of an Mg-Gd alloy [J]. Materials Research Letters, 2020, 8(7): 268-274.
- [98] XIAO Zheng-bing, ZHAO Da-hong, HU Jia-wei, DAI Zhi-jie, XIAO Sun-hang, HU Jia-liang, LAI Jian-ping. First-principles investigation of interface atomic arrangement and segregation behavior of solute elements in Al/TiC

- interface in TiC/2219 composites [J]. Materials Today Communications, 2024, 39: 109311.
- [99] ZHU Sheng-zhi, GE Yi-cheng, LI Li-ya, DU Yong. Chemical segregation mechanism and magnetic properties of Sm₂Co₁₇-based permanent magnets: Experimental investigation and first-principles calculations [J]. Journal of Alloys and Compounds, 2023, 960: 170899.
- [100] LI Zong-bo, FENG Yan, WEN Yu-feng, PENG Xiang, CAI Zhi-yong, PENG Chao-qun, WANG Ri-chu. Ab initio molecular dynamics study on the local structures and solid/liquid interface in liquid Al-Ti and Al-B-Ti alloys [J]. Materials Today Communications, 2024, 39: 109290.
- [101] FENG Yun, FENG Yan, LI Zong-bo, PENG Hai-long. Chemically ordered structure and dynamics in Al₈₀Ti₂₀ liquids [J]. Computational Materials Science, 2023, 226: 112256.
- [102] CHEN Si-yuan, LI Song, MA Jiang, YU Hai-bin, LIU Hua-shan, PENG Hai-long. Ultrasonic vibration accelerated aging in La-based bulk metallic glasses [J]. Journal of Non-Crystalline Solids, 2020, 535: 119967.
- [103] LI Hong-kuan, LIU Hua-shan, PENG Hai-long. Atomic dynamics under oscillatory shear in metallic glasses [J]. Journal of Non-Crystalline Solids, 2020, 539: 120069.
- [104] LIU Yang, LIU Hua-shan, PENG Hai-long. Pinning effect on the correlations of nonaffine displacement in metallic glasses [J]. Journal of Non-Crystalline Solids, 2023, 601: 122052.
- [105] ZHANG Chi, FENG Yun, LIU Hua-shan, SZABÓ S, HOLLAND-MORITZ D, EVENSON Z, YANG Fan, PENG Hai-long. Local structures and undercooling ability of Zr—Ti melts [J]. Journal of Non-Crystalline Solids, 2023, 613: 122348.
- [106] JUAN Yong-fei, NIU Guo-shuai, YANG Yang, XU Zi-han, YANG Jian, TANG Wen-qi, JIANG Hai-tao, HAN Yan-feng, DAI Yong-bing, ZHANG Jiao, SUN Bao-de. Accelerated design of Al-Zn-Mg-Cu alloys via machine learning [J]. Transactions of Nonferrous Metals Society of China, 2024, 34(3): 709-723.
- [107] ZUO Zi-bin, ZHU Rong-bo, LIU Xin-yang, CHEN Xiu-ming, SHI Teng-teng, LEI Xia-jun, WU Jian, JIANG Wen-long, YANG Bin, XU Bao-qiang, LUO Huan. Separation of arsenic and antimony: A comprehensive theoretical and experimental study [J]. Journal of Materials Research and Technology, 2024, 31: 1080–1090.
- [108] LI Zong-bo, LI Ya-xing, FENG Yan, FENG Y, WEN Yu-feng, WANG Ri-chu, PENG Chao-qun, CAI Zhi-yong. Ab initio molecular dynamics study of the local structures and migration behaviors of liquid Sb-based alloys [J]. Journal of Physics D: Applied Physics, 2024, 57(11): 115303.
- [109] ZHANG Chen-tong, SHENG Wang, HUANG Liu-qing, ZHANG Sa, ZHANG Yao-hao, CAI Hua-qiang, MENG Jin-shui, LUO Xue-tao. Vanadium as an impurity trapper for purification of metallurgical-grade silicon [J]. Separation and Purification Technology, 2021, 260: 118199.
- [110] CHEN Kun, CHEN Xiu-hua, LEI Yun, MA Wen-hua, HAN Jia-xian, YANG Zi-heng. Mechanism of enhancing B removal from Si with V addition using AlSi as the refining solvent [J]. Separation and Purification Technology, 2018, 203: 168–177.

高纯锑的制备技术研究进展

栗宗波^{1,2}, 冯 艳^{1,2}, 温玉锋³, 王日初^{1,2}, 彭 翔^{1,2}

- 1. 中南大学 材料科学与工程学院,长沙 410083;
- 2. 中南大学 高强结构材料科学与技术国家重点实验室,长沙 410083;
 - 3. 井冈山大学 数学科学与物理学院, 吉安 343000

摘 要:高纯度锑(Sb)是半导体和光伏等行业的必需品,推动了对其生产的研究。本文综述了高纯锑生产和制备技术的研究进展。根据不同的原材料,介绍了生产高纯锑的3种工艺流程。讨论了真空蒸馏的各种工艺参数、区域精炼提纯技术以及高纯锑领域的研究进展。重点介绍了数值模拟、原子尺度模拟以及合金元素在高纯锑领域的研究进展。研究表明,对于锑中难去除的砷元素,在区域精炼过程中加入AI可以更有效地降低砷含量。最后,对高纯锑的提纯进行了总结,为实现高效、环保的高纯锑生产提供了启示,并指出了未来的发展方向。 关键词:高纯锑;制备技术;纯化;偏析

(Edited by Wei-ping CHEN)